Los Alamos NATIONAL LABORATORY EST.1943

LA-UR-18-24386 (Accepted Manuscript)

Beryllium capsule implosions at a case-to-capsule ratio of 3.7 on the National Ignition Facility

Zylstra, Alex; Yi, Sunghwan; MacLaren, S.; Kline, John L.; Kyrala, George Amine; Ralph, J.E.; Bae, J.; Batha, Steven H.; Callahan, D.; Flippo, Kirk Adler; Huang, H.; Hurricane, O.; Khan, S.F.; Kabadi, N.; Kong, C.; Kot, Lynn; Lahmann, B.; Loomis, Eric Nicholas; Masse, L.P.; Millot, M.; Moore, A.; et al.

Provided by the author(s) and the Los Alamos National Laboratory (2019-02-20).

To be published in: Physics of Plasmas

DOI to publisher's version: 10.1063/1.5041285

Permalink to record: http://permalink.lanl.gov/object/view?what=info:lanl-repo/lareport/LA-UR-18-24386

Disclaimer:
Approved for public release. Los Alamos National Laboratory, an affirmative action/equal opportunity employer, is operated by the Los Alamos National Security, LLC for the National Nuclear Security Administration of the U.S. Department of Energy under contract DE-AC52-06NA25396. Los Alamos National Laboratory strongly supports academic freedom and a researcher's right to publish; as an institution, however, the Laboratory does not endorse the viewpoint of a publication or guarantee its technical correctness.

RESEARCH LIBRARY

AIP Publishing

This manuscript was accepted by Phys. Plasmas. Click here to see the version of record.

Beryllium capsule implosions at a case-to-capsule ratio of 3.7 on the National Ignition Facility

A.B. Zylstra,[1, a)] S.A. Yi,[1] S. MacLaren,[2] J. Kline,[1] G. Kyrala,[1] J.E. Ralph,[2] J. Bae,[3] S. Batha,[1] D. Callahan,[2] K. Flippo,[1] H. Huang,[3] O. Hurricane,[2] S.F. Khan,[2] N. Kabadi,[4] C. Kong,[3] L.B. Kot,[1] B. Lahmann,[4] E.N. Loomis,[1] L.P. Masse,[2] M. Millot,[2] A. Moore,[2] A. Nikroo,[2] T.S. Perry,[1] N. Rice,[3] J. Salmonson,[2] R. Shah,[1] H. Sio,[4] M. Stadermann,[2] D.J. Strozzi,[2] R. Tipton,[2] and H. Xu[3]

[1)] *Los Alamos National Laboratory, Los Alamos, NM 87545*
[2)] *Lawrence Livermore National Laboratory, Livermore, CA 94550*
[3)] *General Atomics, San Diego, CA 92186*
[4)] *Massachusetts Institute of Technology, Cambridge, MA 02139*

Beryllium is a candidate ablator material for indirect-drive inertial confinement fusion experiments, motivated by its high mass ablation rate, which is advantageous for implosion coupling efficiency and stabilization of the ablation-front instability growth. We present new data on the shock propagation, in-flight shape, and hot spot self emission shape from gas-filled capsules that demonstrate the feasibility of predictable, symmetric, controllable beryllium implosions at a case-to-capsule ratio of 3.7. The implosions are round (Legendre mode 2 amplitude $\lesssim 5\%$) at an inner beam power and energy fraction of $26-28\%$ of the total, indicating that larger beryllium capsules could be driven symmetrically using the National Ignition Facility.

ACCEPTED MANUSCRIPT

I. INTRODUCTION

Inertial Confinement Fusion (ICF) seeks to create a burning, or 'ignited', plasma, which requires heating and compressing the fuel to exceed the ideal ignition temperature and Lawson criterion[1], which is the product of pressure and energy confinement time ($p\tau$). ICF heats and compresses the plasma by spherical implosion of a spherical shell of fuel, where a 'hot spot' is generated at the center[2]. The fuel is layered inside a shell of 'ablator' material, which absorbs radiation incident upon its outer surface. At a laser driver facility this the radiation is either direct laser illumination (laser direct drive) or by laser-generated x rays (laser indirect drive). The outer surface ablates outwards, accelerating the remaining shell and fuel inwards. Recent ignition experiments at the National Ignition Facility (NIF)[3] have achieved some self heating[4], using implosion designs with increased ablative stabilization[5,6], but ignition is still elusive.

Beryllium has long been a candidate ablator material for ignition experiments due to several advantages over carbon-based ablators[7,8]. Compared to plastic, beryllium has a lower opacity and higher mass density, leading to higher ablation rates[9–11] (mass per unit area and time for a given radiation temperature), which is advantageous for the implosion rocket efficiency and for ablative stabilization[12]. Low ablation-front instability growth factors for beryllium implosions have recently been demonstrated[13]. These properties of beryllium may be advantageous for nominal implosion designs, or enable designs in a different part of the parameter space, for example at lower radiation temperature. Possible disadvantages of beryllium include additional ablated plasma filling the hohlraum and instabilities from microstructure within the coated capsule[14]. The ablation velocity is also reduced as dopant materials, typically copper, are added to the ablator as a preheat shield.

Recent experiments have begun to use beryllium ablators on the NIF, but performance of the initial implosions was dominated by hohlraum-induced drive asymmetries, due to the use of a high-gas-fill hohlraum[15] and small case-to-capsule ratio (CCR)[16]. Small CCR designs have improved energy coupling to the capsule but poor control of the symmetry. Increasing the hohlraum size for a given capsule restores control over the implosion symmetry, but the reduced energy coupling to the capsule, and lower radiation temperature for a given laser energy and power, reduces theoretical performance. Larger CCR designs can use near-vacuum[17,18] or low-gas-fill[19] hohlraums, which are more predictable and have reduced laser backscatter. In this paper, we develop a beryllium implosion platform at a CCR of 3.7 using a low-gas-fill hohlraum, which reduces modeling uncertainty due to the hohlraum relative to small CCR high-gas-fill designs, and will enable experiments to study the unique capsule physics aspects of beryllium. While this CCR is conservative, it is smaller than other recent results using beryllium ablators on NIF[20].

Implosion designs on the NIF are studied using several tuning platforms[21]. The early epoch of the radiation drive launches multiple shocks through the ablator and fuel layer; the symmetry and timing of the shocks are measured using the VISAR velocimetry diagnostic[22] in the keyhole platform[23,24]. The main drive then accelerates the shell to its peak velocity, which occurs at a convergence ratio (CR) of ~ 4. The in-flight symmetry and implosion velocity are measured with backlit radiography using a pinhole imaging camera[25–27], the '2DConA' platform[28], or a 1-D streaked velocity measurement[29]. Lastly, gas-filled capsules without the fuel layer are imploded to measure the stagnation hot-spot symmetry at CR ~ 20, the 'SymCap' platform[30].

In this paper, we describe new data using these plat-

[a)] Electronic mail: zylstra1@llnl.gov

This manuscript was accepted by Phys. Plasmas. Click here to see the version of record.

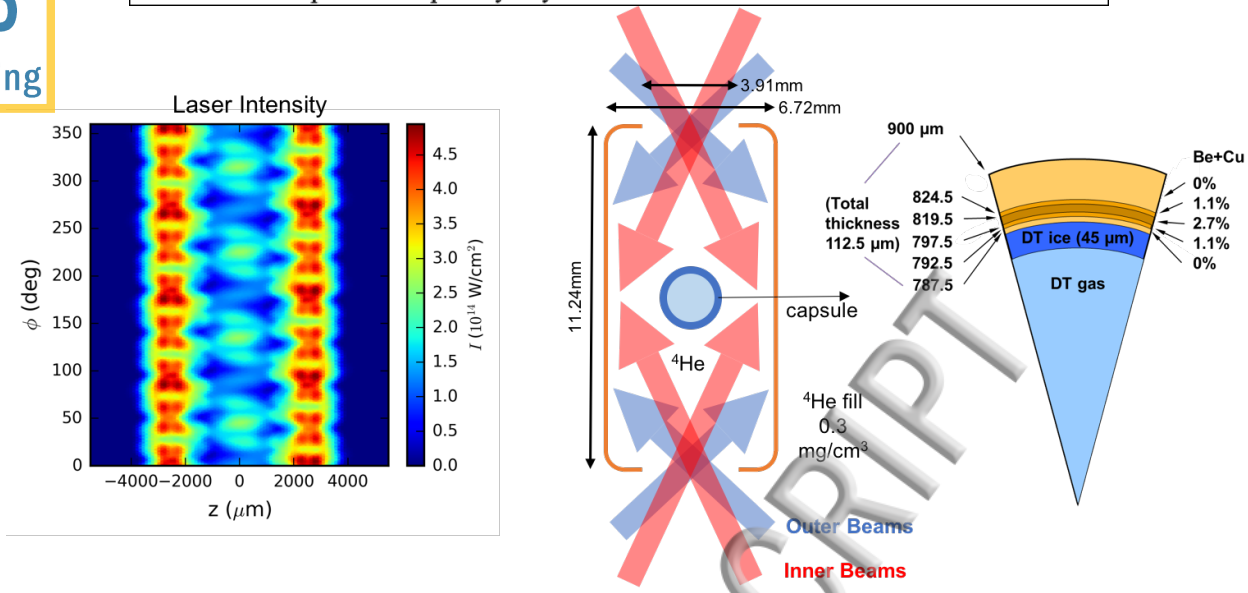

FIG. 1: CCR=3.7 beryllium target design. Center: hohlraum dimensions and target geometry, left: laser intensity on the hohlraum wall, right: capsule dimensions.

forms to study beryllium ablator implosions at a conservative CCR of 3.7. The data demonstrate predictable control over the implosion symmetry. The paper is organized as follows: Section II describes the design parameters chosen for these experiments, Section III describes our simulation methodology, Section IV presents the shock timing and symmetry data, Section V describes the implosion symmetry measurements, Section VI presents the stagnation performance data, and the paper is concluded in Section VII

II. BERYLLIUM PLATFORM

The beryllium implosion target design used in this paper is shown in Fig. 1. The hohlraum is 6.72mm in diameter ('672'), 11.24mm in length, with 3.91mm diameter laser entrance holes (LEH), and 30μm thick Au walls. The hohlraum is filled with 0.3 mg/cm^3 of ^{4}He gas, referred to as a low-gas-fill (LGF) hohlraum. The capsule is 900 μm in outer radius, 112.5 μm thick, with graded layers of copper-doped beryllium, up to 2.7% atomic Cu, as a preheat shield. The solid (ice) DT fuel in a layered implosion is nominally 45 μm thick. For 2DConA and SymCap experiments, the ice layer is replaced by a 6 μm thick surrogate layer of extra Be. For keyhole experiments, the capsule is filled with liquid D_2.

The laser pointing scheme is chosen to minimize the flux asymmetries on the capsule. The four 'cones' of NIF beams are pointed at $z = \pm 3.606$ mm (23° beams), $z = \pm 4.24$ mm (30° beams), $z = \pm 5.523$ mm (45° beams), and $z = \pm 5.775$ mm (50° beams). The outer beams (45° and 50° beams) within a quad are split azimuthally. The resulting laser intensity on the hohlraum wall is shown in Fig. 1, calculated using VISRAD[31].

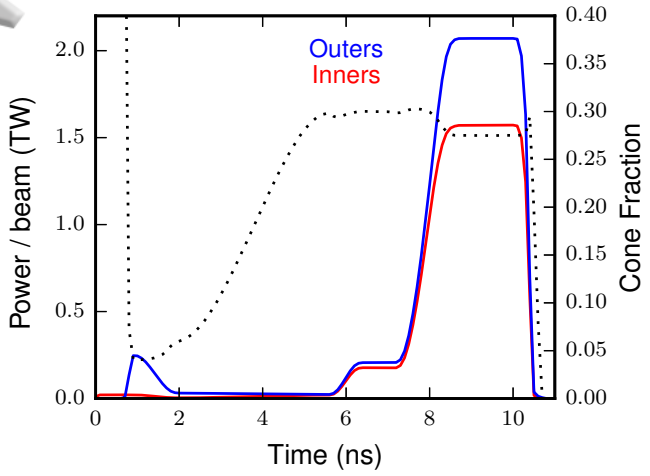

FIG. 2: Nominal laser pulse, showing the inner beam (red) and outer beam (blue) pulses. The cone fraction (dotted curve, right axis) is 27.5% during the main pulse in this instance.

A nominal laser pulse shape is shown in Fig. 2. This platform uses a 3-shock design similar to recent high-adiabat campaigns using CH[5,32] and HDC[33] ablators. The first shock, launched by the picket in the outer cone beam power at $\sim$ 1 ns, is $\sim$ 3 MBar in order to ensure that the beryllium melts[34]. The picket is preceded by a small amount of power on the inner beams to burn through the LEH window. The example pulse shape uses a 27.5% cone fraction (CF, ratio of inner power to total power); over this series of experiments the CF is adjusted

ACCEPTED MANUSCRIPT

This manuscript was accepted by Phys. Plasmas. Click here to see the version of record.

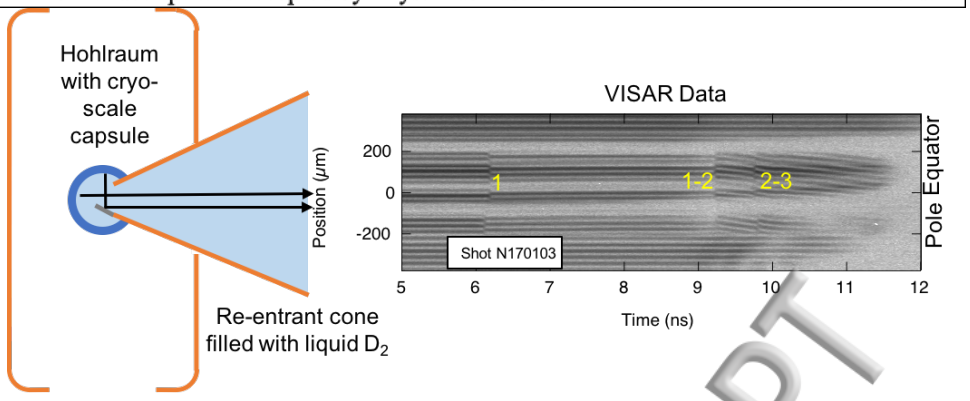

FIG. 3: Shock timing configuration (left); a re-entrant cone inserted into the capsule allows a reflected probe beam to measure the shock velocity using interferometry. Right: example interferometry data from shot N170103 showing fringe shifts associated with the first shock ($\sim$ 6 ns), 1-2 merger ($\sim$ 9 ns), and 2-3 merger ($\sim$ 10 ns).

by changing the outer beam and inner beam power during peak power while conserving the total energy and power. Lower CFs give a pole-hot drive that results in a more oblate implosion. This pulse shape is a total of 1MJ of energy with a peak power of 370 TW, significantly less than the full NIF capabilities (1.8MJ, 500TW) because of the small capsule.

Overall, this implosion design is relatively conservative on CCR (3.7) and velocity ($\sim 330 - 340$ km/s) and has a nominally long coast time[35] ($\sim$ 1.6 ns), but is more aggressive on implosion adiabat than other recent campaigns. Adiabat is defined as the ratio of the in-flight (at peak velocity) dense fuel pressure to the cold (zero temperature) pressure, $\alpha \equiv P/P_{cold} \sim 2$. The adiabat is directly related to the average fuel entropy, and is calculated from simulations following the prescription in Ref. 36.

III. SIMULATION METHODOLOGY

Each shot is modeled using 2-D radiation-hydrodynamics simulations using the actual target dimensions and laser delivery. Measured laser backscatter is removed from the incident power. Integrated calculations including both the hohlraum and capsule are conducted using the `HYDRA`[37] code. Multipliers are applied during the picket, trough, and second shock launch parts of the pulse, plus the peak of the drive, in order to match the shock timing data and the observed emission peak from the implosion stagnation (bang time)[38]. A detailed configuration accounting (DCA) model is used in the hohlraum similar to Ref. 38 and a flux limiter of 0.15 is applied to the electron conductivity model in the hohlraum. In order to match the data, no multiplier (i.e. 1.0×) is needed in the picket and trough, while a 0.8× multiplier in the second shock launch and a 0.9× multiplier during the peak pulse are required. Additionally, a CF multiplier of 1.07×, i.e. increasing the inner beam power by 7% and decreasing the outer beam power by a corresponding amount, is needed to match the implosion symmetry. The same set of multipliers is used to model every shot. The multipliers may be needed to account for physics uncertainty in the hohlraum model or the capsule microphysics, such as using a tabular beryllium equation of state instead of a first-principles calculation[39]. These simulations are post-processed to generate synthetic data for direct comparison to the measured values in the following sections.

IV. SHOCK TIMING AND SYMMETRY

Control over the spherical symmetry, velocity, and merger times of the shocks launched are key for achieving high performance of an ICF capsule implosion[21]. We use the standard 'keyhole' platform[23], which is shown schematically in Fig. 3, for these measurements. A re-entrant cone is placed through the hohlraum and capsule wall, and the capsule and cone are filled with liquid D_2. The probe laser for the VISAR interferometer[23] enters through a window in the cone and reflects back into the interferometer. Views at the capsule equator and pole are obtained simultaneously in a mirrored configuration. The probe beam initially reflects off of the inner capsule surface, and then from the shock front once it breaks out from the beryllium into the liquid D_2. Example data from shot N170103 are shown in Fig. 3, the timing and velocity of the shocks are determined by the fringe shifts.

The measured shock velocity versus time is shown in Fig. 4 from the pole (red) and equator (blue). Two shots are shown. On top is N170103, where the three shocks are seen sequentially: the first shock breaks out from the beryllium at $\sim$ 6 ns, is overtaken by the second shock at $\sim$ 9 ns, and the 1-2 merged shock is finally overtaken by the third shock at $\sim$ 10 ns. On shot N170410 (bottom of Fig. 4), the first shock breaks out at around the same time, but the second and third shocks merge before the second overtakes the first, and therefore the third shock

ACCEPTED MANUSCRIPT

This manuscript was accepted by Phys. Plasmas. Click here to see the version of record.

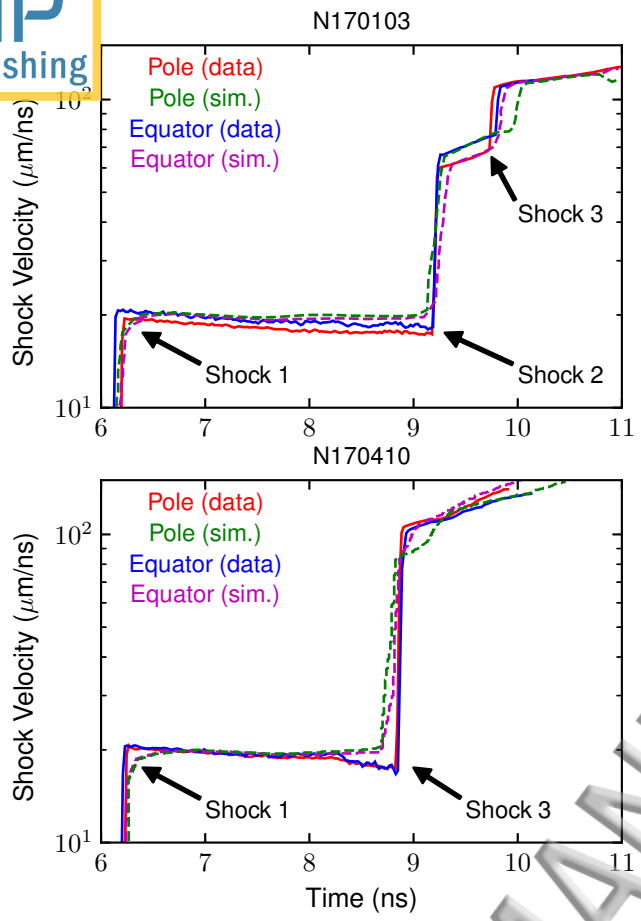

FIG. 4: Shock velocity versus time for two shots: N170103 (top) and N170410 (bottom). On N170103 the three shocks are seen sequentially, while on N170410 the second and third shocks were intentionally merged before they catch the first shock.

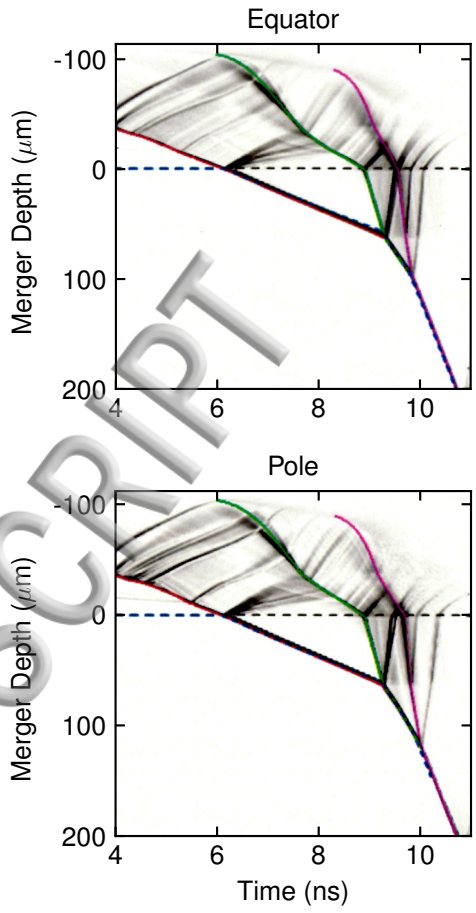

FIG. 5: Simulated shock trajectories showing log P in grayscale versus radius (relative to the interface) and time for the equator (top) and pole (bottom) on shot N170103.

is next seen in the interferometer data at $\sim$ 9 ns. The shock timing of the laser pulse is intentionally changed to create these configurations.

The shock velocity versus time and break-out/merger times are very similar between the polar and equatorial data, within $\pm$80 ps, demonstrating good shock symmetry. The simulated values are shown by the green dashed (polar) and purple dashed (equatorial). The simulations agree well with the data after a 0.8$\times$ multiplier is applied to the radiation flux on the capsule during the second shock launch, as described in Section III. The simulated shock trajectories for shot N170103 are also visualized in Fig. 5 as the pressure (grayscale) versus radius and time on both the equator and pole. The multiplier inferred from this data will be used to adjust the shock timing for subsequent implosions using fuel layers in this platform.

V. IMPLOSION SYMMETRY

Control over the symmetry of an implosion is also critical for high performance[21], as deviation from sphericity degrades the stagnation in several ways. The implosion symmetry is measured using two techniques: in-flight, using area-backlit x-ray radiography and pinhole camera imaging (the '2DConA' platform[28]), and by measuring the stagnation plasma x-ray self-emission (the 'SymCap' platform[30]). In both cases capsules with a several mg/cm^3 fill of D_2 or D_2+^{3}He gas are used instead of DT fuel layers. The mass of the nominal design's DT fuel layer (see Fig. 1) is replaced by an equivalent mass of beryllium ablator material to mimic the total payload mass.

An experimental schematic for the 2DConA x-ray radiography is shown in Fig. 6. Two of the NIF quads (31T and 26B) drive a Cu backlighter foil to radiograph the in-flight shell. An example image from shot N170314 is shown at the right, where the capsule has imploded to

ACCEPTED MANUSCRIPT

This manuscript was accepted by Phys. Plasmas. Click here to see the version of record.

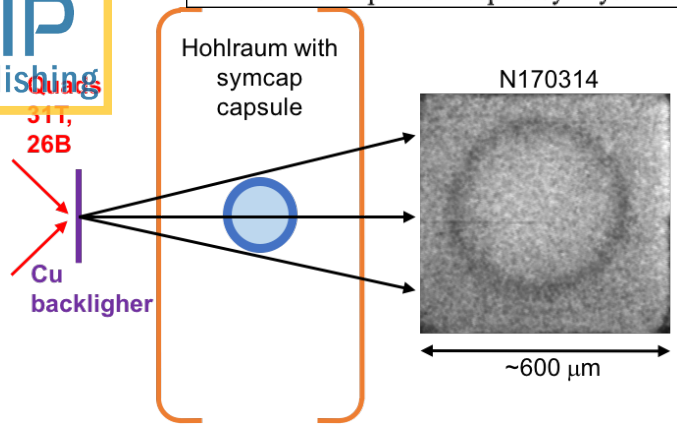

FIG. 6: Cartoon of the x-ray radiography experiments. Two quads (31T and 26B) drive a Cu backlighter foil, producing an area x-ray backlighter. At right is an example in-flight radiograph from shot N170314 showing the shell at a radius of ~ 200 μm.

a radius ~ 200 μm, roughly corresponding to peak velocity and a convergence ratio (CR, initial inner radius to final radius) of ~ 4. The shell symmetry at this time is evaluated by analyzing the shell absorption in the radiograph.

As the shell stagnates and converts the implosion kinetic energy into internal energy in the fuel, the hot spot x-ray emission is imaged using x-ray pinhole cameras. In these gas-filled capsules, the CR is typically $\sim 12-20$ depending on the gas fill density. Example images are shown in Fig. 7 from shot N170327, showing the x-ray emission at peak brightness ('bang time') imaged at the pole and equator.

The implosion symmetry is analyzed by fitting a series of Legendre modes to the observed shape. The polar mode 2 (P_2) asymmetry is a primary focus of these tuning campaigns as low-mode drive asymmetries are not symmeterized by the hohlraum and must be controlled. P_2 is typically tuned by adjusting the relative powers of the inner and outer beam cones[30] (see Fig. 1), where the cone fraction (CF) is defined as the ratio of the inner cone power to the total.

A pair of 2DConA implosions were shot where only the cone fraction was varied. These shots used the nominal total drive (1.0MJ, 370TW, see Fig. 2), and are plotted against the as-delivered cone fraction during the peak of the drive. The in-flight symmetry is typically reported at a radius $P_0 \sim 200$ μm while the stagnation data are measured at bang time; these data are shown in Fig.

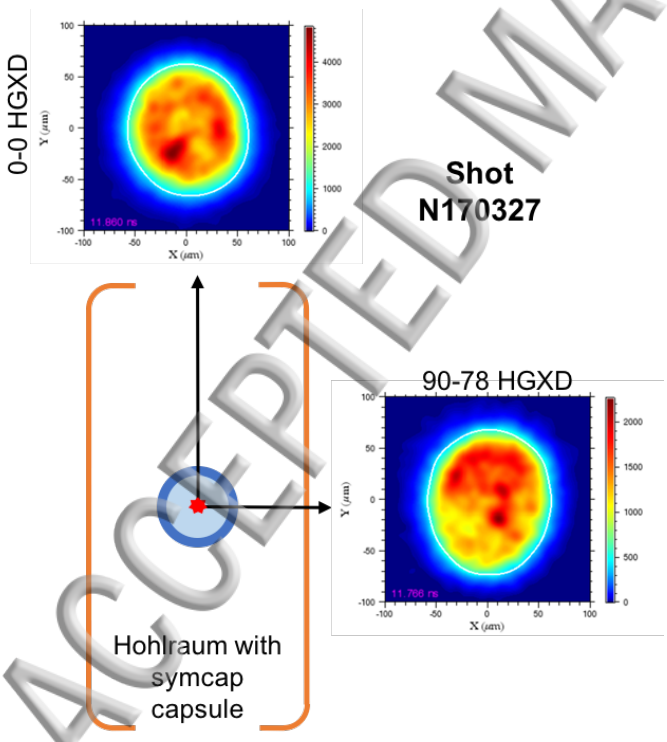

FIG. 7: In the gas-filled 'SymCap' capsules, the x-ray emission at stagnation is imaged using pinhole cameras at the pole and equator. Example data from shot N170327 are shown.

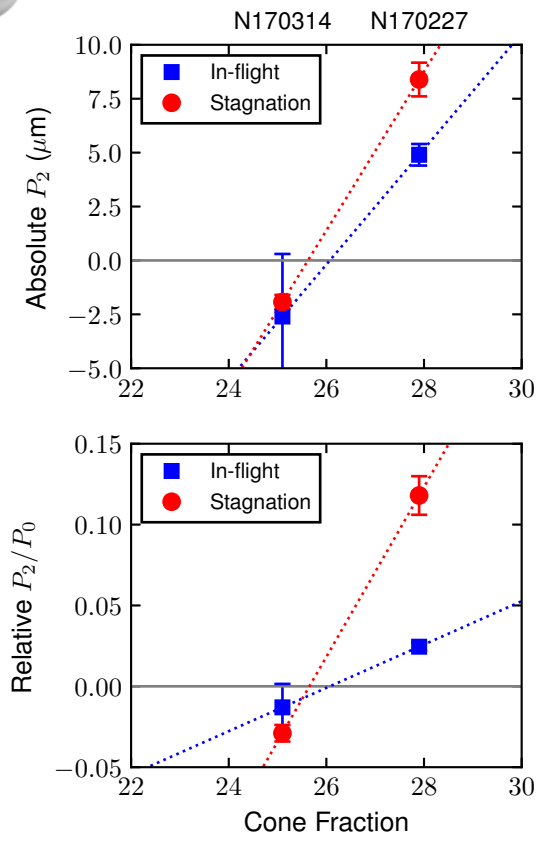

FIG. 8: Polar mode 2 (P_2) symmetry versus cone fraction, plotted as absolute (top) and relative (bottom) amplitude, while the implosion is in-flight (blue squares) and at stagnation (red points).

ACCEPTED MANUSCRIPT

This manuscript was accepted by Phys. Plasmas. Click here to see the version of record.

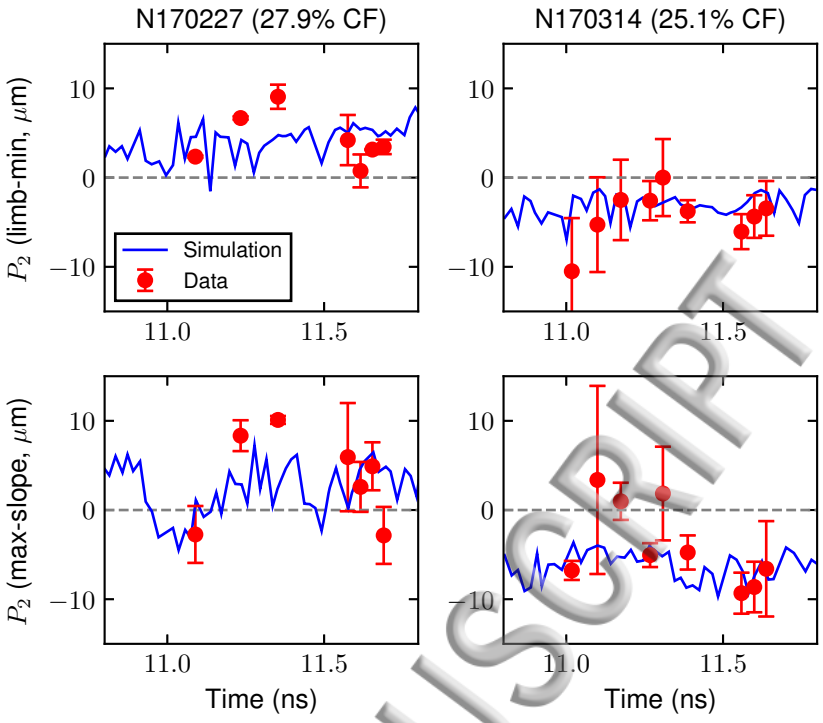

FIG. 9: P_2 (limb minimum, top; maximum slope, bottom) versus time for N170227 (left) and N170314 (right).

8. The top plot shows the absolute magnitude of the P_2 asymmetry while the bottom plot shows the relative asymmetry magnitude (P_2/P_0). The dashed curves are linear fits to the data. The data show that the implosion would be round, both in flight and at stagnation, for a cone fraction of $\sim 26\%$.

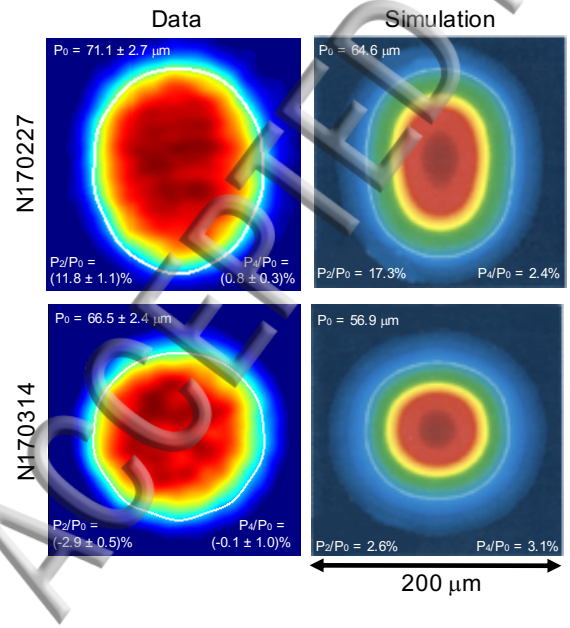

FIG. 10: Bang-time self-emission images [N170227 (top), N170314 (bottom)], with data (left) compared to simulation (right).

A detailed comparison of the in-flight symmetry is shown in Fig. 9. Each pinhole image from the area-backlit radiography is analyzed to give a time sequence of P_2 values, which are taken from either the maximum slope or limb minimum of the imploding shell's absorption in the image[28]. For these shots, the measurement uncertainty and variation between subsequent measurements are often large due to the relatively low contrast of the images compared to typical implosions.

Results from the post-shot `HYDRA` simulations are also shown in Fig. 9 (blue curves), and show qualitatively good agreement with the data given the experimental measurement variability and uncertainty. These simulations continue to the implosion stagnation; a bang time self-emission synthetic x-ray image is calculated from the simulation and compared to data in Fig. 10. The stagnation images are measured to higher precision allowing detailed quantitative comparison. The mode 2 shape (P_2/P_0) is 5.5% more oblate than predicted by the simulation. The apparent size (P_0) is also smaller in the simulation by 8 μm. The simulated images are more strongly peaked at the center, reducing the size of the 17% contour used to calculate P_0.

ACCEPTED MANUSCRIPT

This manuscript was accepted by Phys. Plasmas. Click here to see the version of record.

V. STAGNATION PERFORMANCE

To further test the platform, we conducted a series of SymCap implosions where the capsule gas fill, laser energy, and cone fraction were varied to test the predictability of these implosions to changes in convergence ratio and drive characteristics. The shots are summarized in Table I. This experimental series was designed to test the effect of increased convergence ratio on the shape (N170327 → N170406), which is sensitive to swings in the time-dependent drive symmetry. We also tested the effect of an extended ('no-coast') pulse with peak power continued for an additional 800ps (N170406 → N170503), and the effect of cone fraction symmetry tuning with the pulse extension (N170503 → N170530). Unlike the 2DConA backlit-radiography experiments described in the previous section, which used 6.3 mg/cc of a D_2+^{3}He gas mixture (30:70 atomic) as the capsule fill, these SymCap experiments used 2.0 or 4.0 mg/cc of pure D_2.

TABLE I: SymCap series

Shot	Gas Fill (mg/cm^3)	Laser Energy (MJ)	Cone Fraction (%)
N170327	4	1.0	27.5
N170406	2	1.0	27.5
N170503	2	1.3	27.5
N170530	2	1.3	30.5

In these experiments the primary shape diagnostic is the equatorial self-emission imaging[27], which is shown in Fig. 11. The first shot, N170327 (top row), is directly comparable to N170227 as they are both shot at the same cone fraction and energy. The capsule has converged slightly more with the lower mass density fill, and the shape is equivalent within measurement uncertainty. On N170406 (second row), the gas mass density was decreased to 2mg/cc, which is intended to increase the implosion convergence ratio further. The apparent x-ray self-emission image is equivalent in shape but only slightly smaller than N170327. This is because the inner region of the shell material starts to emit x rays in addition to the hot spot.

On shot N170503 (third row) the pulse duration was then extended by 800ps at the same cone fraction as N170406. Late in the pulse the inner beams are increasingly absorbed in the outer beam's gold blowoff bubble rather than on the hohlraum waist, which tends to create a pole-hot drive later in time[40,41]. This manifests as a more oblate implosion on N170503. The inner beam power is then increased to a cone fraction of 30.5%, keeping the total power and energy constant, on N170530, which results in a ∼ 20% prolate implosion (lower right). The simulations (right column of Fig. 11) closely match the observed shape data for all four shots.

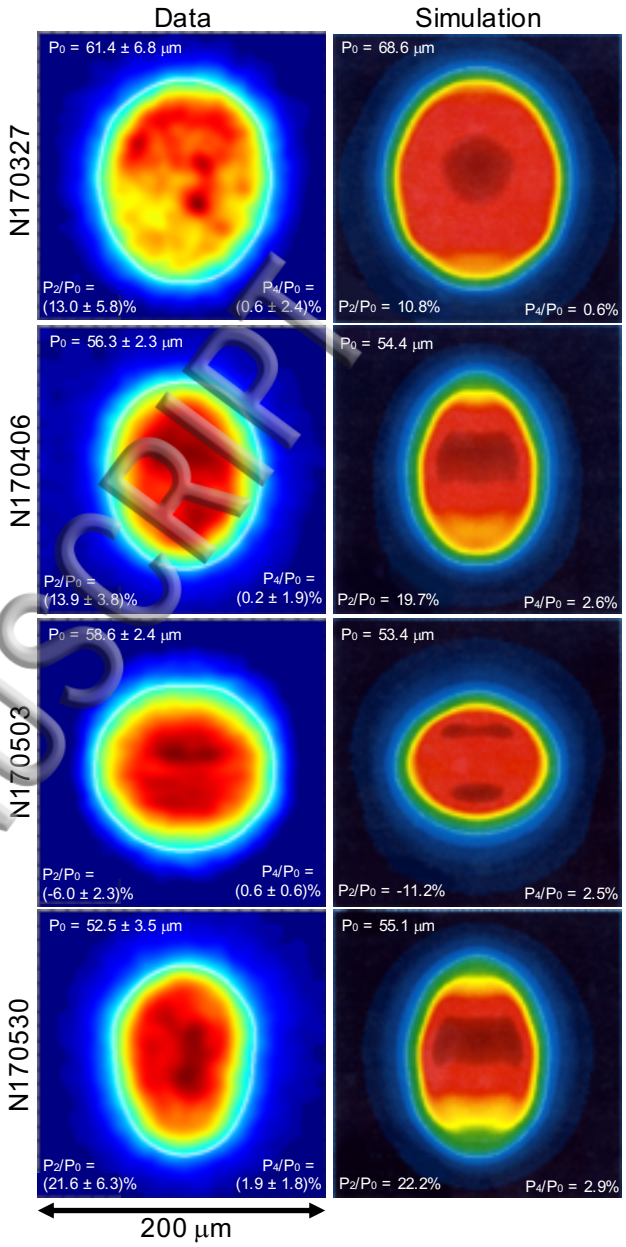

FIG. 11: Equatorial x-ray self-emission at bang time for the SymCap shot series. Data are shown at left, simulated images at the right.

Since these SymCap implosions used a purely hydrogenic fuel (unlike the 2DConAs, which were majority ^{3}He) the clean fuel's x-ray emissivity is reduced, making the emission images more sensitive to injected high-Z material. The images in Fig. 11 show bright features, which are partly due to injected high-Z material from the fill tube jet. At peak emission, when the hot spot volume is small, the bright features from the fill tube can be less clearly resolved (as in Fig. 11). Images earlier in time clearly show the injected material from the fill tube, see Appendix C.

ACCEPTED MANUSCRIPT

This manuscript was accepted by Phys. Plasmas. Click here to see the version of record.

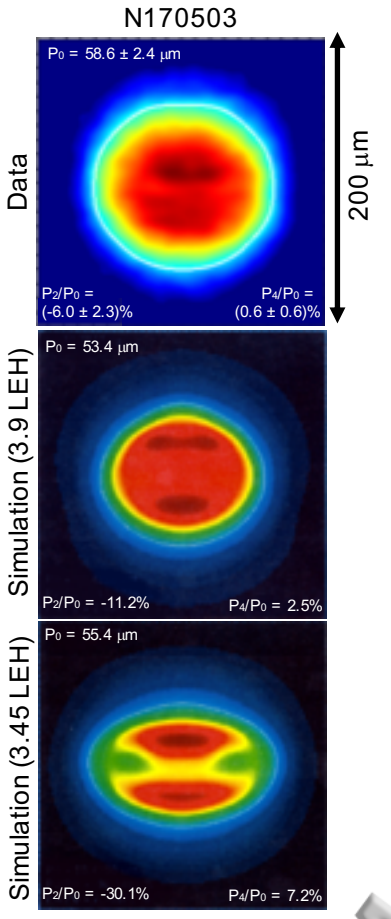

FIG. 12: Equatorial x-ray self-emission data for shot N170503 (top) compared to HYDRA simulations using the incorrect LEH size (3.9mm), which matches the shape, and the actual LEH size (3.45mm) which is significantly more oblate in the calculation.

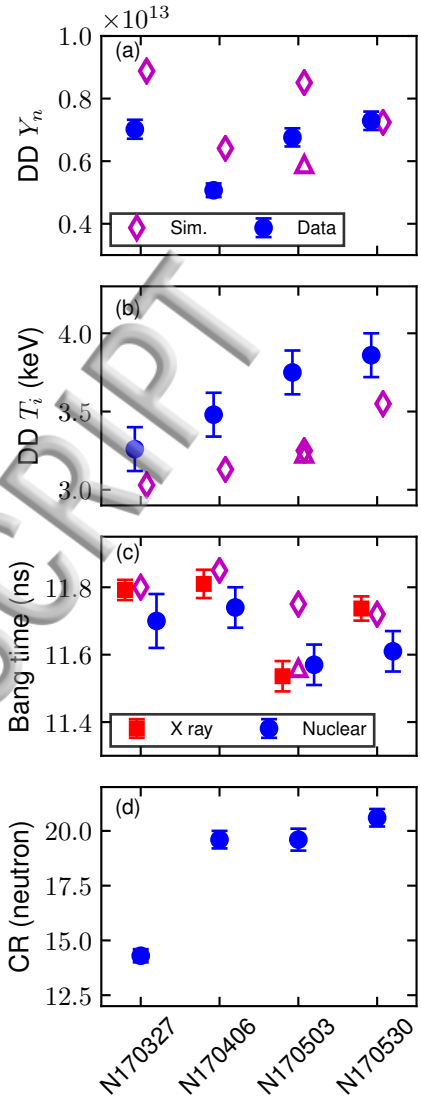

FIG. 13: Nuclear data from the SymCap series: total yield (a), burn-averaged ion temperature (T_i, b), bang time (c), and convergence ratio (CR) inferred from secondary neutrons (d). Both x-ray (red squares) and nuclear (blue points) bang times are shown in (c). Simulations are shown by the magenta diamonds. For shot N170503, the simulation with 3.45mm LEH is shown by the magenta triangle.

The shape data are potentially affected by an inadvertent change in the LEH size on N170503. The LEH size is defined by an 'insert' washer; the incorrect part was installed on this shot with an inner diameter of 3.45mm instead of the nominal 3.9mm (see Fig. 1). While this increased the overall drive sufficiently to noticeably advance the implosion bang time, post-shot simulations indicate that the shape change observed relative to N170406 and N17530 is dominated by the pulse extension and a slight picket energy over delivery. The simulation shown in Fig. 11 used the nominal LEH size, yet matches the shape well. When the smaller LEH size (3.45mm) is included, the simulation is significantly more oblate than the data (see Fig. 12). These shots seem to indicate that the HYDRA simulations capture the increase in drive due to the LEH size change, as evidenced by the earlier bang time, but significantly over-predict the effect on the drive symmetry. Auxiliary data related to this, including soft x-ray imaging[42] and drive diagnostics[43,44], are discussed in Appendices A and B.

These data show that the implosion shape is well determined by systematic changes in parameters such as the cone fraction and pulse duration. With the extended pulse, these shots show that a cone fraction of $\sim 28\%$ is needed for a symmetric implosion. While higher than the $\sim 26\%$ found in the previous section for the standard duration pulse, this is still significantly less than the natural 33% cone fraction on NIF.

Nuclear data are also collected from the D+D fusion

ACCEPTED MANUSCRIPT

This manuscript was accepted by Phys. Plasmas. Click here to see the version of record.

reaction:

$$\mathrm{D} + \mathrm{D} \rightarrow \mathrm{T}\ (1.01\ \mathrm{MeV}) + \mathrm{p}\ (3.02\ \mathrm{MeV}), \quad (1)$$
$$\rightarrow {}^{3}\mathrm{He}\ (0.82\ \mathrm{MeV}) + \mathrm{n}\ (2.45\ \mathrm{MeV}). \quad (2)$$

The total yield of neutrons from Eq. 2 and their thermal Doppler width, thus ion temperature (T_i), is measured using time-of-flight detectors[45,46]. The x-ray bang time is measured using a streak camera system[47], and the neutron bang time is measured with a diamond-based detector[48]. Finally, the implosion convergence ratio (CR) is inferred by measuring the secondary 14.1 MeV DT neutron, produced by in-flight reactions of the triton from Eq. 1. The secondary to primary yield ratio is related to the fuel areal density[49], and thus convergence. These data are shown in Fig. 13. A direct comparison to simulations would require charged-particle transport of the tritons and has not been done for the simulations presented in this work.

As the gas density is halved, the yield decreases by about 30% as it is partly compensated by the increased convergence and T_i (N170327 $\rightarrow$ N170406). As the coast time is decreased using the extended pulse, we see a clear increase in the yield and T_i, consistent with an increased hot-spot pressure from the late-time drive[35]. Simulated values are shown in Fig. 13 by the magenta diamonds. The simulated yield-over-clean (YOC) is about $80-100\%$, which is typical for moderate-convergence gas-filled implosions. The simulated temperature underestimates the data by about 300eV. The bang times typically match well, except for N170503 when simulated with the 3.9mm LEH (which matches the shape). When using a 3.45mm LEH the simulation matches the bang time (Fig. 13) but cannot match the shape (Fig. 12).

VII. CONCLUSIONS

Beryllium, as an ablator material, has advantageous implosion efficiency and ablation-front stabilization due to its high mass ablation velocity, but has not been extensively tested on the NIF, unlike plastic and high-density carbon ablators. In this work, we have benchmarked the performance of beryllium implosions at a case-to-capsule ratio of 3.7. We find that the implosions are predictable with controllably symmetry through shock, implosion, and stagnation. The stagnation symmetry sensitivity to convergence ratio, pulse duration, and cone fraction has been measured using gas-filled capsules. These data will be used to design DT layered implosions in this platform to test the stagnation performance relative to expectations, in a system where the hohlraum is predictable and controllable (unlike Ref. 15).

We find that these implosions are round at cone fractions of $26-28\%$, significantly less than the natural 33% operating point for NIF. This demonstrates that larger beryllium capsules could be fielded in this hohlraum[40]. Such 'full-scale' designs, with capsule sizes $\sim 20\%$ larger than those considered in this work (CCR ~ 3), would operate in a parameter space comparable to recent high-performing designs using CH and HDC ablators; the potential performance of such designs will be evaluated using simulations.

ACKNOWLEDGMENTS

We thank the operations, engineering, and target fabrication staff at NIF for supporting these experiments. This work was performed under the auspices of the U.S. DoE by LANL under contract DE-AC52-06NA52396, by LLNL under contract DE-AC52-07NA27344, and by GA under contract DE-NA0001808.

Appendix A: SXI data

Soft x-ray emission through the LEH is measured by the Static X-ray Imager (SXI)[42] on NIF. This instrument is fielded at target-chamber coordinates $(\theta, \phi) = (18, 123)$. The data from our four-shot SymCap series (Table I and Fig. 11) are shown in Fig. 14.

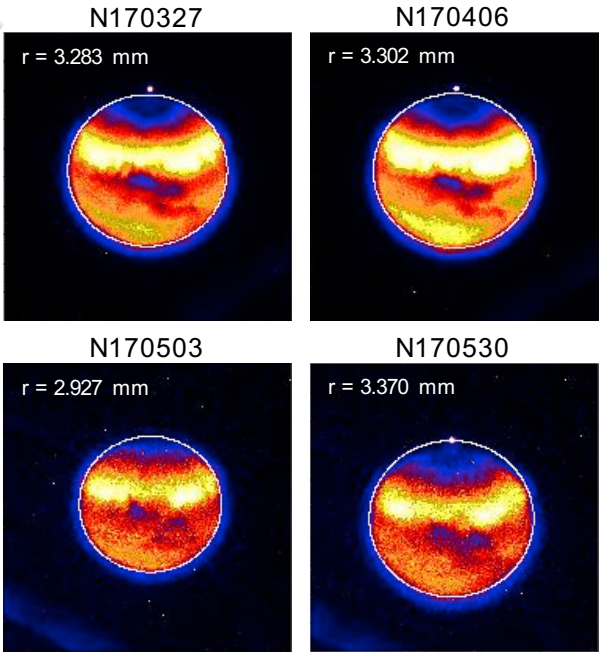

FIG. 14: Soft x-ray emission through the LEH at an angle of 18° to the axis. A fit to the clear aperture (white curve) gives a measurement of the LEH size, including closure.

The white circles and quoted radii correspond to the time-integrated clear aperture. The LEH size decreases from the initial size due to closure - the edges ablate and Au plasma moves towards the axis. On N170327, N170406, and N170530 the measured sizes are consistent.

ACCEPTED MANUSCRIPT

This manuscript was accepted by Phys. Plasmas. Click here to see the version of record.

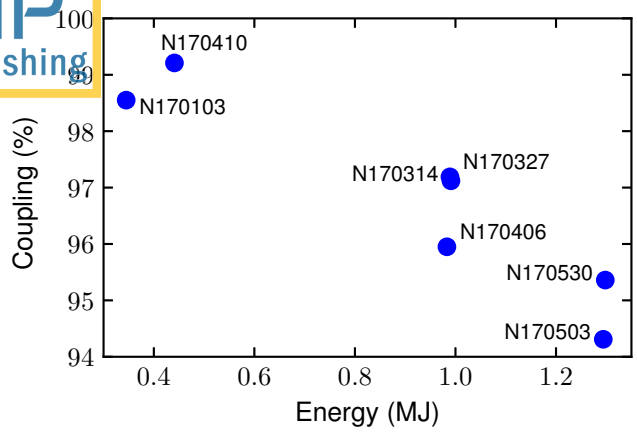

FIG. 15: Measured laser coupling versus laser energy. Data were not acquired for N170227.

The LEH size on N170503 is $\sim 10\%$ smaller, consistent with the inadvertent small-LEH target built for that shot.

Appendix B: Drive diagnostics

As the lasers propagate to the hohlraum wall, various laser-plasma instabilities (LPI) can reduce the overall coupling to the hohlraum. For these low-gas-fill hohlraums, coupling is typically high[17,19]. The NIF backscatter suite of diagnostics[50] are used to measure coupling on these experiments. The data are shown in Fig. 15 for all shots except N170227, which had a diagnostic configuration problem. The keyhole experiments, at low energy, have a coupling near 99%. The ~ 1 MJ 2DConA and SymCap experiments (N170314, N170327, and N170406) have a coupling near $96 - 97\%$. On the 1.3MJ SymCaps (N170503 and N170530), the coupling decreases slightly to $\sim 95\%$.

Additionally, the absolute thermal radiation flux and temperature are measured by a soft x-ray spectrometer Dante[43,44,51]. The measured radiation temperatures versus time, in the second shock and main peak parts of the drive, are shown in Fig. 16. The laser pulse power versus time is also shown.

Appendix C: Fill tube

The capsules used for implosion experiments on the NIF are typically fueled through a small borosilicate glass tube called the 'fill tube', which is inserted through a hole drilled in the capsule and attached with a fillet of glue. It is well known that the hydrodynamic evolution of the fill tube can create a jet of material into the hot spot[52,53], which typically manifests itself as a bright feature seen in gas-filled or layered implosion hot spot self-emission images.

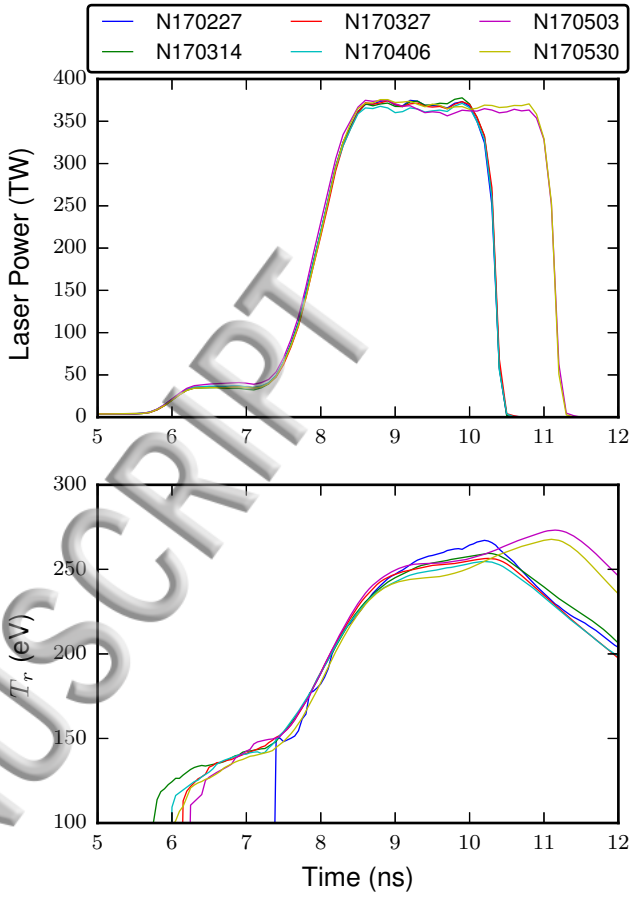

FIG. 16: Delivered laser pulse (top) and measured radiation temperature (T_r, bottom) for the six 2DConA and SymCap experiments.

Fig. 17 shows self-emission hot-spot images from the pole (top) and equator (bottom) approximately 150ps before bang time for our four SymCap shots. Cartoons of the experimental geometry are shown to the right of Fig. 17. In the polar view, the fill tube is oriented towards the lower left of the images. A bright emission feature, typical of the fill tube, is observed in each image. Similarly, in the equatorial view the fill tube is oriented away from the camera and to the right, and a bright emission feature is observed in each image. These data may aid in interpreting the relative impact of such engineering features on the performance of different ablator materials[53].

Appendix D: Shot setup details

This Appendix contains detailed shot setup information on the reported experiments. The shots and their specific target and laser details are summarized in Table II.

Both keyhole experiments (N170103 and N170410) were fielded at 21.5 °K and filled with liquid D_2. The

ACCEPTED MANUSCRIPT

This manuscript was accepted by Phys. Plasmas. Click here to see the version of record.

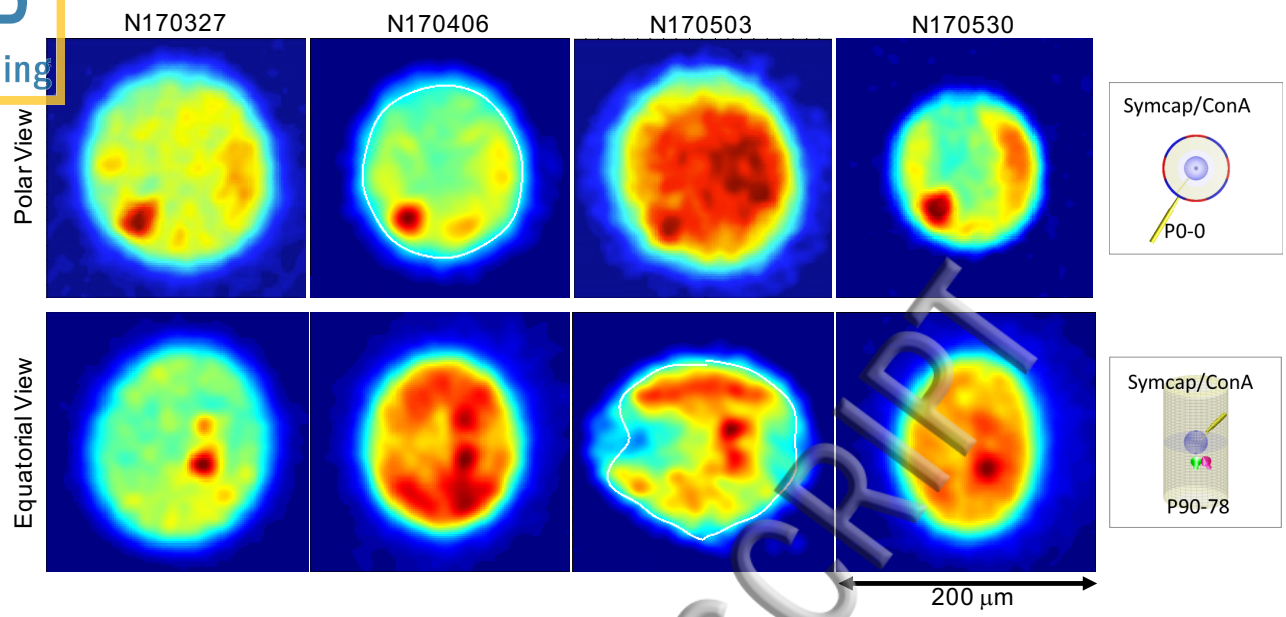

FIG. 17: X-ray hot-spot self emission measured ∼ 150 ps before bang time on the pole (top) and equator (bottom) for the four SymCap experiments. At right, a cartoon shows the experimental geometry including the fill tube location.

2DConA shots (N170227 and N170314) were fielded at 24 °K and filled with 6.3 mg/cc of D_2+^{3}He gas, with atomic fractions of 30 and 70% respectively. The SymCaps were fielded at 32 °K and filled with either 4 or 2 mg/cc of pure D_2 gas.

The 2DConA and SymCap targets used a standard capsule support and filling scheme, with 45nm thick tents and 10 μm diameter fill tubes.

ACCEPTED MANUSCRIPT

[1]J. D. Lawson, Proceedings of the Physical Society. Section B **70**, 6 (1957).
[2]J. Nuckolls, L. Wood, A. Thiessen, and G. Zimmerman, Nature **239**, 139–142 (1972).
[3]G. Miller, E. Moses, and C. Wuest, Nuclear Fusion **44**, S228 (2004).
[4]O. Hurricane, D. Callahan, D. Casey, P. Celliers, C. Cerjan, E. Dewald, T. Dittrich, T. Döppner, D. Hinkel, L. Berzak Hopkins, J. Kline, S. Le Pape, T. Ma, A. MacPhee, J. Milovich, A. Pak, H.-S. Park, P. Patel, B. Remington, J. Salmonson, P. Springer, and R. Rommasini, Nature **506**, 343 (2014).
[5]T. R. Dittrich, O. A. Hurricane, D. A. Callahan, E. L. Dewald, T. Döppner, D. E. Hinkel, L. F. Berzak Hopkins, S. Le Pape, T. Ma, J. L. Milovich, J. C. Moreno, P. K. Patel, H.-S. Park, B. A. Remington, J. D. Salmonson, and J. L. Kline, Phys. Rev. Lett. **112**, 055002 (2014).
[6]H.-S. Park, O. A. Hurricane, D. A. Callahan, D. T. Casey, E. L. Dewald, T. R. Dittrich, T. Döppner, D. E. Hinkel, L. F. Berzak Hopkins, S. Le Pape, T. Ma, P. K. Patel, B. A. Remington, H. F. Robey, J. D. Salmonson, and J. L. Kline, Phys. Rev. Lett. **112**, 055001 (2014).
[7]T. R. Dittrich, S. W. Haan, S. Pollaine, A. K. Burnham, and G. L. Strobel, Fusion Technology **31**, 402–405 (1997).
[8]D. C. Wilson, P. A. Bradley, N. M. Hoffman, F. J. Swenson, D. P. Smitherman, R. E. Chrien, R. W. Margevicius, D. J. Thoma, L. R. Foreman, J. K. Hoffer, S. R. Goldman, S. E. Caldwell, T. R. Dittrich, S. W. Haan, M. M. Marinak, S. M. Pollaine, and J. J. Sanchez, Phys. Plasmas **5**, 1953–1959 (1998).
[9]R. E. Olson, G. A. Rochau, O. L. Landen, and R. J. Leeper, Phys. Plasmas **18**, 032706 (2011).
[10]D. T. Michel, V. N. Goncharov, I. V. Igumenshchev, R. Epstein, and D. H. Froula, Phys. Rev. Lett. **111**, 245005 (2013).
[11]D. T. Casey, D. T. Woods, V. A. Smalyuk, O. A. Hurricane, V. Y. Glebov, C. Stoeckl, W. Theobald, R. Wallace, A. Nikroo, M. Schoff, C. Shuldberg, K. J. Wu, J. A. Frenje, O. L. Landen, B. A. Remington, and G. Glendinning, Phys. Rev. Lett. **114**, 205002 (2015).
[12]H. Takabe, K. Mima, L. Montierth, and R. L. Morse, The Physics of Fluids **28**, 3676–3682 (1985).
[13]S. A. Yi, A. N. Simakov, D. C. Wilson, R. E. Olson, J. L. Kline, D. S. Clark, B. A. Hammel, J. L. Milovich, J. D. Salmonson, B. J. Kozioziemski, and S. H. Batha, Phys. Plasmas **21**, 092701 (2014).
[14]H. W. Xu, C. S. Alford, J. C. Cooley, L. A. Dixon, R. E. Hackenberg, S. A. Letts, K. A. Moreno, A. Nikroo, J. R. Wall, and K. P. Youngblood, Fusion Science and Technology **51**, 547–552 (2007), http://dx.doi.org/10.13182/FST51-547.
[15]J. L. Kline, S. A. Yi, A. N. Simakov, R. E. Olson, D. C. Wilson, G. A. Kyrala, T. S. Perry, S. H. Batha, A. B. Zylstra, E. L. Dewald, R. Tommasini, J. E. Ralph, D. J. Strozzi, A. G. MacPhee, D. A. Callahan, D. E. Hinkel, O. A. Hurricane, J. L. Milovich, J. R. Rygg, S. F. Khan, S. W. Haan, P. M. Celliers, D. S. Clark, B. A. Hammel, B. Kozioziemski, M. B. Schneider, M. M. Marinak, H. G. Rinderknecht, H. F. Robey, J. D. Salmonson, P. K. Patel, T. Ma, M. J. Edwards, M. Stadermann, S. Baxamusa, C. Alford, M. Wang, A. Nikroo, N. Rice, D. Hoover, K. P. Youngblood, H. Xu, H. Huang, and H. Sio, Phys. Plasmas **23**, 056310 (2016).
[16]A. N. Simakov, D. C. Wilson, S. A. Yi, E. N. Loomis, J. L. Kline, G. A. Kyrala, A. B. Zylstra, E. L. Dewald, R. Tommasini, J. E. Ralph, D. J. Strozzi, A. G. MacPhee, J. L. Milovich, J. R. Rygg, S. F. Khan, T. Ma, L. C. Jarrott, S. W. Haan, P. M. Celliers, M. M. Marinak, H. G. Rinderknecht, H. F. Robey, J. D. Salmonson, M. Stadermann, S. Baxamusa, C. Alford, Y. Wang, A. Nikroo, N. Rice, C. Kong, J. Jaquez, M. Mauldin, K. P. Youngblood, H. Xu, H. Huang, and H. Sio, Phys. Plasmas **24**,

This manuscript was accepted by Phys. Plasmas. Click here to see the version of record.

TABLE II: Shot setup parameters

Shot	N170103 -002	N170227 -001	N170314 -001	N170327 -002	N170406 -003	N170410 -001	N170503 -003	N170530 -002
Type	Keyhole	2DConA	2DConA	SymCap	SymCap	Keyhole	SymCap	SymCap
Capsule								
Batch	S2NIF736	S6NIF352	S6NIF352	S6NIF354	S6NIF354	S2NIF736	S6NIF354	S6NIF354
OR (μm)	908.5	908.4	904.7	903.5	903.4	906.2	905.8	906.1
Thick. (μm)	114.3	122.5	119.6	116.7	116.6	114.3	117.0	116.6
Laser								
Total Energy (MJ)	0.345	0.989	0.991	0.989	0.983	0.441	1.294	1.298
Peak Power (TW)	194.3	374.7	377.7	374.3	371.2	250.1	374.8	375.6
Picket Energy (kJ)	23.4	22.0	23.3	23.3	23.6	22.4	26.7	22.8
Cone Fraction (%)	30.9	27.9	25.1	27.9	27.9	31.1	28.3	30.8
Duration (ns)	9.8	10.5	10.5	10.5	10.5	9.4	11.3	11.3

ACCEPTED MANUSCRIPT

052704 (2017).
[17]L. F. Berzak Hopkins, N. B. Meezan, S. Le Pape, L. Divol, A. J. Mackinnon, D. D. Ho, M. Hohenberger, O. S. Jones, G. Kyrala, J. L. Milovich, A. Pak, J. E. Ralph, J. S. Ross, L. R. Benedetti, J. Biener, R. Bionta, E. Bond, D. Bradley, J. Caggiano, D. Callahan, C. Cerjan, J. Church, D. Clark, T. Döppner, R. Dylla-Spears, M. Eckart, D. Edgell, J. Field, D. N. Fittinghoff, M. Gatu Johnson, G. Grim, N. Guler, S. Haan, A. Hamza, E. P. Hartouni, R. Hatarik, H. W. Herrmann, D. Hinkel, D. Hoover, H. Huang, N. Izumi, S. Khan, B. Kozioziemski, J. Kroll, T. Ma, A. MacPhee, J. McNaney, F. Merrill, J. Moody, A. Nikroo, P. Patel, H. F. Robey, J. R. Rygg, J. Sater, D. Sayre, M. Schneider, S. Sepke, M. Stadermann, W. Stoeffl, C. Thomas, R. P. J. Town, P. L. Volegov, C. Wild, C. Wilde, E. Woerner, C. Yeamans, B. Yoxall, J. Kilkenny, O. L. Landen, W. Hsing, and M. J. Edwards, Phys. Rev. Lett. **114**, 175001 (2015).
[18]N. B. Meezan, L. F. B. Hopkins, S. L. Pape, L. Divol, A. J. MacKinnon, T. Dppner, D. D. Ho, O. S. Jones, S. F. Khan, T. Ma, J. L. Milovich, A. E. Pak, J. S. Ross, C. A. Thomas, L. R. Benedetti, D. K. Bradley, P. M. Celliers, D. S. Clark, J. E. Field, S. W. Haan, N. Izumi, G. A. Kyrala, J. D. Moody, P. K. Patel, J. E. Ralph, J. R. Rygg, S. M. Sepke, B. K. Spears, R. Tommasini, R. P. J. Town, J. Biener, R. M. Bionta, E. J. Bond, J. A. Caggiano, M. J. Eckart, M. G. Johnson, G. P. Grim, A. V. Hamza, E. P. Hartouni, R. Hatarik, D. E. Hoover, J. D. Kilkenny, B. J. Kozioziemski, J. J. Kroll, J. M. McNaney, A. Nikroo, D. B. Sayre, M. Stadermann, C. Wild, B. E. Yoxall, O. L. Landen, W. W. Hsing, and M. J. Edwards, Phys. Plasmas **22**, 062703 (2015).
[19]L. Divol, A. Pak, L. F. B. Hopkins, S. L. Pape, N. B. Meezan, E. L. Dewald, D. D.-M. Ho, S. F. Khan, A. J. Mackinnon, J. S. Ross, D. P. Turnbull, C. Weber, P. M. Celliers, M. Millot, L. R. Benedetti, J. E. Field, N. Izumi, G. A. Kyrala, T. Ma, S. R. Nagel, J. R. Rygg, D. Edgell, A. G. Macphee, C. Goyon, M. Hohenberger, B. J. MacGowan, P. Michel, D. Strozzi, W. Cassata, D. Casey, D. N. Fittinghoff, N. Gharibyan, R. Hatarik, D. Sayre, P. Volegov, C. Yeamans, B. Bachmann, T. Dppner, J. Biener, J. Crippen, C. Choate, H. Huang, C. Kong, A. Nikroo, N. G. Rice, M. Stadermann, S. D. Bhandarkar, S. Haan, B. Kozioziemski, W. W. Hsing, O. L. Landen, J. D. Moody, R. P. J. Town, D. A. Callahan, O. A. Hurricane, and M. J. Edwards, Phys. Plasmas **24**, 056309 (2017).
[20]E. N. Loomis, S. A. Yi, G. A. Kyrala, J. Kline, A. Simakov, J. Ralph, M. Millot, E. Dewald, A. Zylstra, J. R. Rygg, P. Celliers, C. Goyon, B. Lahmann, H. Sio, S. MacLaren, L. Masse, D. Callahan, O. Hurricane, D. C. Wilson, N. Rice, H. Huang, C. Kong, J. Bae, A. Nikroo, and S. H. Batha, Phys. Plasmas **25**, 072708 (2018).
[21]M. J. Edwards, P. K. Patel, J. D. Lindl, L. J. Atherton, S. H. Glenzer, S. W. Haan, J. D. Kilkenny, O. L. Landen, E. I. Moses, A. Nikroo, R. Petrasso, T. C. Sangster, P. T. Springer, S. Batha, R. Benedetti, L. Bernstein, R. Betti, D. L. Bleuel, T. R. Boehly, D. K. Bradley, J. A. Caggiano, D. A. Callahan, P. M. Celliers, C. J. Cerjan, K. C. Chen, D. S. Clark, G. W. Collins, E. L. Dewald, L. Divol, S. Dixit, T. Doeppner, D. H. Edgell, J. E. Fair, M. Farrell, R. J. Fortner, J. Frenje, M. G. G. Johnson, E. Giraldez, V. Y. Glebov, G. Grim, B. A. Hammel, A. V. Hamza, D. R. Harding, S. P. Hatchett, N. Hein, H. W. Herrmann, D. Hicks, D. E. Hinkel, M. Hoppe, W. W. Hsing, N. Izumi, B. Jacoby, O. S. Jones, D. Kalantar, R. Kauffman, J. L. Kline, J. P. Knauer, J. A. Koch, B. J. Kozioziemski, G. Kyrala, K. N. LaFortune, S. L. Pape, R. J. Leeper, R. Lerche, T. Ma, B. J. MacGowan, A. J. MacKinnon, A. Macphee, E. R. Mapoles, M. M. Marinak, M. Mauldin, P. W. McKenty, M. Meezan, P. A. Michel, J. Milovich, J. D. Moody, M. Moran, D. H. Munro, C. L. Olson, K. Opachich, A. E. Pak, T. Parham, H.-S. Park, J. E. Ralph, S. P. Regan, B. Remington, H. Rinderknecht, H. F. Robey, M. Rosen, S. Ross, J. D. Salmonson, J. Sater, D. H. Schneider, F. H. Sguin, S. M. Sepke, D. A. Shaughnessy, V. A. Smalyuk, B. K. Spears, C. Stoeckl, W. Stoeffl, L. Suter, C. A. Thomas, R. Tommasini, R. P. Town, S. V. Weber, P. J. Wegner, K. Widman, M. Wilke, D. C. Wilson, C. B. Yeamans, and A. Zylstra, Phys. Plasmas **20**, 070501 (2013).
[22]R. M. Malone, B. C. Frogget, M. I. Kaufman, T. W. Tunnell, R. L. Guyton, I. P. Reinbachs, P. W. Watts, J. R. Celeste, P. M. Celliers, T. L. Lee, B. J. MacGowan, E. W. Ng, R. B. Robinson, and L. G. Seppala, in *International Optical Design Conference* (Optical Society of America, 2006) p. ThA5.
[23]H. F. Robey, P. M. Celliers, J. L. Kline, A. J. Mackinnon, T. R. Boehly, O. L. Landen, J. H. Eggert, D. Hicks, S. Le Pape, D. R. Farley, M. W. Bowers, K. G. Krauter, D. H. Munro, O. S. Jones, J. L. Milovich, D. Clark, B. K. Spears, R. P. J. Town, S. W. Haan, S. Dixit, M. B. Schneider, E. L. Dewald, K. Widmann, J. D. Moody, T. D. Döppner, H. B. Radousky, A. Nikroo, J. J. Kroll, A. V. Hamza, J. B. Horner, S. D. Bhandarkar, E. Dzenitis, E. Alger, E. Giraldez, C. Castro, K. Moreno, C. Haynam, K. N. LaFortune, C. Widmayer, M. Shaw, K. Jancaitis, T. Parham, D. M. Holunga, C. F. Walters, B. Haid, T. Malsbury, D. Trum-

This manuscript was accepted by Phys. Plasmas. Click here to see the version of record.

ner, K. R. Coffee, B. Burr, L. V. Berzins, C. Choate, S. J. Brereton, S. Azevedo, H. Chandrasekaran, S. Glenzer, J. A. Caggiano, P. M. Bell, J. P. Knauer, J. A. Frenje, D. T. Casey, M. Gatu Johnson, F. H. Séguin, B. K. Young, M. J. Edwards, B. M. Van Wonterghem, J. Kilkenny, B. J. MacGowan, J. Atherton, J. D. Lindl, D. D. Meyerhofer, and E. Moses, Phys. Rev. Lett. **108**, 215004 (2012).

[24]J. D. Moody, H. F. Robey, P. M. Celliers, D. H. Munro, D. A. Barker, K. L. Baker, T. Dppner, N. L. Hash, L. B. Hopkins, K. LaFortune, O. L. Landen, S. LePape, B. J. MacGowan, J. E. Ralph, J. S. Ross, C. Widmayer, A. Nikroo, E. Giraldez, and T. Boehly, Phys. Plasmas **21**, 092702 (2014).

[25]J. A. Oertel, R. Aragonez, T. Archuleta, C. Barnes, L. Casper, V. Fatherley, T. Heinrichs, R. King, D. Landers, F. Lopez, P. Sanchez, G. Sandoval, L. Schrank, P. Walsh, P. Bell, M. Brown, R. Costa, J. Holder, S. Montelongo, and N. Pederson, Rev. Sci. Instrum. **77**, 10E308 (2006).

[26]D. Hargrove, J. Holder, N. Izumi, L. Benedetti, G. Stone, J. Kimbrough, P. Bell, and S. Glenn, in *Proc. SPIE*, Vol. 9211 (2014) p. 92110D.

[27]L. R. Benedetti, J. P. Holder, M. Perkins, C. G. Brown, C. S. Anderson, F. V. Allen, R. B. Petre, D. Hargrove, S. M. Glenn, N. Simanovskaia, D. K. Bradley, and P. Bell, Rev. Sci. Instrum. **87**, 023511 (2016).

[28]J. R. Rygg, O. S. Jones, J. E. Field, M. A. Barrios, L. R. Benedetti, G. W. Collins, D. C. Eder, M. J. Edwards, J. L. Kline, J. J. Kroll, O. L. Landen, T. Ma, A. Pak, J. L. Peterson, K. Raman, R. P. J. Town, and D. K. Bradley, Phys. Rev. Lett. **112**, 195001 (2014).

[29]D. G. Hicks, N. B. Meezan, E. L. Dewald, A. J. Mackinnon, R. E. Olson, D. A. Callahan, T. Dppner, L. R. Benedetti, D. K. Bradley, P. M. Celliers, D. S. Clark, P. D. Nicola, S. N. Dixit, E. G. Dzenitis, J. E. Eggert, D. R. Farley, J. A. Frenje, S. M. Glenn, S. H. Glenzer, A. V. Hamza, R. F. Heeter, J. P. Holder, N. Izumi, D. H. Kalantar, S. F. Khan, J. L. Kline, J. J. Kroll, G. A. Kyrala, T. Ma, A. G. MacPhee, J. M. McNaney, J. D. Moody, M. J. Moran, B. R. Nathan, A. Nikroo, Y. P. Opachich, R. D. Petrasso, R. R. Prasad, J. E. Ralph, H. F. Robey, H. G. Rinderknecht, J. R. Rygg, J. D. Salmonson, M. B. Schneider, N. Simanovskaia, B. K. Spears, R. Tommasini, K. Widmann, A. B. Zylstra, G. W. Collins, O. L. Landen, J. D. Kilkenny, W. W. Hsing, B. J. MacGowan, L. J. Atherton, and M. J. Edwards, Phys. Plasmas **19**, 122702 (2012).

[30]G. A. Kyrala, J. L. Kline, S. Dixit, S. Glenzer, D. Kalantar, D. Bradley, N. Izumi, N. Meezan, O. Landen, D. Callahan, S. V. Weber, J. P. Holder, S. Glenn, M. J. Edwards, J. Koch, L. J. Suter, S. W. Haan, R. P. J. Town, P. Michel, O. Jones, S. Langer, J. D. Moody, E. L. Dewald, T. Ma, J. Ralph, A. Hamza, E. Dzenitis, and J. Kilkenny, Phys. Plasmas **18**, 056307 (2011).

[31]J. MacFarlane, Journal of Quantitative Spectroscopy and Radiative Transfer **81**, 287–300 (2003).

[32]D. E. Hinkel, L. F. Berzak Hopkins, T. Ma, J. E. Ralph, F. Albert, L. R. Benedetti, P. M. Celliers, T. Döppner, C. S. Goyon, N. Izumi, L. C. Jarrott, S. F. Khan, J. L. Kline, A. L. Kritcher, G. A. Kyrala, S. R. Nagel, A. E. Pak, P. Patel, M. D. Rosen, J. R. Rygg, M. B. Schneider, D. P. Turnbull, C. B. Yeamans, D. A. Callahan, and O. A. Hurricane, Phys. Rev. Lett. **117**, 225002 (2016).

[33]D. Turnbull, L. F. Berzak Hopkins, S. L. Pape, L. Divol, N. Meezan, O. L. Landen, D. D. Ho, A. Mackinnon, A. B. Zylstra, H. G. Rinderknecht, H. Sio, R. D. Petrasso, J. S. Ross, S. Khan, A. Pak, E. L. Dewald, D. A. Callahan, O. Hurricane, W. W. Hsing, and M. J. Edwards, Phys. Plasmas **23**, 052710 (2016).

[34]B. A. Hammel and the National Ignition Campaign Team, Plasma Physics and Controlled Fusion **48**, B497 (2006).

[35]O. A. Hurricane, A. Kritcher, D. A. Callahan, O. Landen, P. K. Patel, P. T. Springer, D. T. Casey, E. L. Dewald, T. R. Dittrich, T. Dppner, D. E. Hinkel, L. F. B. Hopkins, J. Kline, S. L. Pape, T. Ma, A. G. MacPhee, A. Moore, A. Pak, H.-S. Park, J. Ralph, J. D. Salmonson, and K. Widmann, Phys. Plasmas **24**, 092706 (2017).

[36]S. W. Haan, J. D. Lindl, D. A. Callahan, D. S. Clark, J. D. Salmonson, B. A. Hammel, L. J. Atherton, R. C. Cook, M. J. Edwards, S. Glenzer, A. V. Hamza, S. P. Hatchett, M. C. Herrmann, D. E. Hinkel, D. D. Ho, H. Huang, O. S. Jones, J. Kline, G. Kyrala, O. L. Landen, B. J. MacGowan, M. M. Marinak, D. D. Meyerhofer, J. L. Milovich, K. A. Moreno, E. I. Moses, D. H. Munro, A. Nikroo, R. E. Olson, K. Peterson, S. M. Pollaine, J. E. Ralph, H. F. Robey, B. K. Spears, P. T. Springer, L. J. Suter, C. A. Thomas, R. P. Town, R. Vesey, S. V. Weber, H. L. Wilkens, and D. C. Wilson, Phys. Plasmas **18**, 051001 (2011).

[37]M. M. Marinak, G. D. Kerbel, N. A. Gentile, O. Jones, D. Munro, S. Pollaine, T. R. Dittrich, and S. W. Haan, Phys. Plasmas **8**, 2275–2280 (2001).

[38]O. S. Jones, C. J. Cerjan, M. M. Marinak, J. L. Milovich, H. F. Robey, P. T. Springer, L. R. Benedetti, D. L. Bleuel, E. J. Bond, D. K. Bradley, D. A. Callahan, J. A. Caggiano, P. M. Celliers, D. S. Clark, S. M. Dixit, T. Doppner, R. J. Dylla-Spears, E. G. Dzentitis, D. R. Farley, S. M. Glenn, S. H. Glenzer, S. W. Haan, B. J. Haid, C. A. Haynam, D. G. Hicks, B. J. Kozioziemski, K. N. LaFortune, O. L. Landen, E. R. Mapoles, A. J. MacKinnon, J. M. McNaney, N. B. Meezan, P. A. Michel, J. D. Moody, M. J. Moran, D. H. Munro, M. V. Patel, T. G. Parham, J. D. Sater, S. M. Sepke, B. K. Spears, R. P. J. Town, S. V. Weber, K. Widmann, C. C. Widmayer, E. A. Williams, L. J. Atherton, M. J. Edwards, J. D. Lindl, B. J. MacGowan, R. E. Suter, L. J. and, H. W. Herrmann, J. L. Kline, G. A. Kyrala, D. C. Wilson, J. Frenje, T. R. Boehly, V. Glebov, J. P. Knauer, A. Nikroo, H. Wilkens, and J. D. Kilkenny, Phys. Plasmas **19**, 056315 (2012).

[39]Y. H. Ding and S. X.Hu, Phys. Plasmas **24**, 062702 (2017).

[40]D. A. Callahan, O. A. Hurricane, J. E. Ralph, C. A. Thomas, K. L. Baker, L. R. Benedetti, L. F. B. Hopkins, D. T. Casey, T. Chapman, C. E. Czajka, E. L. Dewald, L. Divol, T. Dppner, D. E. Hinkel, M. Hohenberger, L. C. Jarrott, S. F. Khan, A. L. Kritcher, O. L. Landen, S. LePape, S. A. MacLaren, L. P. Masse, N. B. Meezan, A. E. Pak, J. D. Salmonson, D. T. Woods, N. Izumi, T. Ma, D. A. Mariscal, S. R. Nagel, J. L. Kline, G. A. Kyrala, E. N. Loomis, S. A. Yi, A. B. Zylstra, and S. H. Batha, Phys. Plasmas **25**, 056305 (2018).

[41]A. L. Kritcher, D. Clark, S. Haan, S. A. Yi, A. B. Zylstra, D. A. Callahan, D. E. Hinkel, L. F. B. Hopkins, O. A. Hurricane, O. L. Landen, S. A. MacLaren, N. B. Meezan, P. K. Patel, J. Ralph, C. A. Thomas, R. Town, and M. J. Edwards, Phys. Plasmas **25**, 056309 (2018).

[42]M. B. Schneider, O. S. Jones, N. B. Meezan, J. L. Milovich, R. P. Town, S. S. Alvarez, R. G. Beeler, D. K. Bradley, J. R. Celeste, S. N. Dixit, M. J. Edwards, M. J. Haugh, D. H. Kalantar, J. L. Kline, G. A. Kyrala, O. L. Landen, B. J. MacGowan, P. Michel, J. D. Moody, S. K. Oberhelman, K. W. Piston, M. J. Pivovaroff, L. J. Suter, A. T. Teruya, C. A. Thomas, S. P. Vernon, A. L. Warrick, K. Widmann, R. D. Wood, and B. K. Young, Rev. Sci. Instrum. **81**, 10E538 (2010).

[43]J. L. Kline, K. Widmann, A. Warrick, R. E. Olson, C. A. Thomas, A. S. Moore, L. J. Suter, O. Landen, D. Callahan, S. Azevedo, J. Liebman, S. H. Glenzer, A. Conder, S. N. Dixit, P. T. III, V. Tran, E. L. Dewald, J. Kamperschroer, L. J. Atherton, R. B. Jr., L. Berzins, J. Celeste, C. Haynam, W. Hsing, D. Larson, B. J. MacGowan, D. Hinkel, D. Kalantar, R. Kauffman, J. Kilkenny, N. Meezan, M. D. Rosen, M. Schneider, E. A. Williams, S. Vernon, R. J. Wallace, B. V. Wonterghem, and B. K. Young, Rev. Sci. Instrum. **81**, 10E321 (2010).

[44]R. E. Marrs, K. Widmann, G. V. Brown, R. F. Heeter, S. A. MacLaren, M. J. May, A. S. Moore, and M. B. Schneider, Rev. Sci. Instrum. **86**, 103511 (2015).

[45]T. Clancy, J. Caggiano, J. McNaney, M. Eckart, M. Moran, V. Glebov, J. Knauer, R. Hatarik, S. Friedrich, R. Zacharias, A. Carpenter, M. Shoup, M. Buczek, M. Yeoman, Z. Zeid, B. Zaitseva, J. Talison, J. Worden, B. Rice, T. Duffy, A. Pruyne, and K. Marshall, Proc. SPIE **9211** (2014), 10.1117/12.2062329.

ACCEPTED MANUSCRIPT

This manuscript was accepted by Phys. Plasmas. Click here to see the version of record.

[46]R. Hatarik, D. B. Sayre, J. A. Caggiano, T. Phillips, M. J. Eckart, E. J. Bond, C. Cerjan, G. P. Grim, E. P. Hartouni, J. P. Knauer, J. M. Mcnaney, and D. H. Munro, Journal of Applied Physics **118**, 184502 (2015).

[47]S. Khan, P. Bell, D. Bradley, S. Burns, J. Celeste, L. Dauffy, M. Eckart, M. Gerhard, C. Hagmann, D. Headley, J. Holder, N. Izumi, M. Jones, J. Kellogg, H. Khater, J. Kimbrough, A. MacPhee, Y. Opachich, N. Palmer, R. Petre, J. Porter, R. Shelton, T. Thomas, and J. Worden, in *Proc. SPIE*, Vol. 8505 (2012) p. 850505.

[48]H. G. Rinderknecht, M. G. Johnson, A. B. Zylstra, N. Sinenian, M. J. Rosenberg, J. A. Frenje, C. J. Waugh, C. K. Li, F. H. Sguin, R. D. Petrasso, J. R. Rygg, J. R. Kimbrough, A. MacPhee, G. W. Collins, D. Hicks, A. Mackinnon, P. Bell, R. Bionta, T. Clancy, R. Zacharias, T. Dppner, H. S. Park, S. LePape, O. Landen, N. Meezan, E. I. Moses, V. U. Glebov, C. Stoeckl, T. C. Sangster, R. Olson, J. Kline, and J. Kilkenny, Rev. Sci. Instrum. **83**, 10D902 (2012).

[49]H. G. Rinderknecht, M. J. Rosenberg, A. B. Zylstra, B. Lahmann, F. H. Sguin, J. A. Frenje, C. K. Li, M. G. Johnson, R. D. Petrasso, L. F. B. Hopkins, J. A. Caggiano, L. Divol, E. P. Hartouni, R. Hatarik, S. P. Hatchett, S. L. Pape, A. J. Mackinnon, J. M. McNaney, N. B. Meezan, M. J. Moran, P. A. Bradley, J. L. Kline, N. S. Krasheninnikova, G. A. Kyrala, T. J. Murphy, M. J. Schmitt, I. L. Tregillis, S. H. Batha, J. P. Knauer, and J. D. Kilkenny, Phys. Plasmas **22**, 082709 (2015).

[50]J. D. Moody, P. Datte, K. Krauter, E. Bond, P. A. Michel, S. H. Glenzer, L. Divol, C. Niemann, L. Suter, N. Meezan, B. J. MacGowan, R. Hibbard, R. London, J. Kilkenny, R. Wallace, J. L. Kline, K. Knittel, G. Frieders, B. Golick, G. Ross, K. Widmann, J. Jackson, S. Vernon, and T. Clancy, Rev. Sci. Instrum. **81**, 10D921 (2010).

[51]E. L. Dewald, K. M. Campbell, R. E. Turner, J. P. Holder, O. L. Landen, S. H. Glenzer, R. L. Kauffman, L. J. Suter, M. Landon, M. Rhodes, and D. Lee, Rev. Sci. Instrum. **75**, 3759–3761 (2004).

[52]A. G. MacPhee, D. T. Casey, D. S. Clark, S. Felker, J. E. Field, S. W. Haan, B. A. Hammel, J. Kroll, O. L. Landen, D. A. Martinez, P. Michel, J. Milovich, A. Moore, A. Nikroo, N. Rice, H. F. Robey, V. A. Smalyuk, M. Stadermann, and C. R. Weber, Phys. Rev. E **95**, 031204 (2017).

[53]D. Clark, A. Kritcher, S. Yi, A. Zylstra, S. Haan, and C. Weber, Phys. Plasmas **25**, 032703 (2018).

ACCEPTED MANUSCRIPT

ACCEPTED

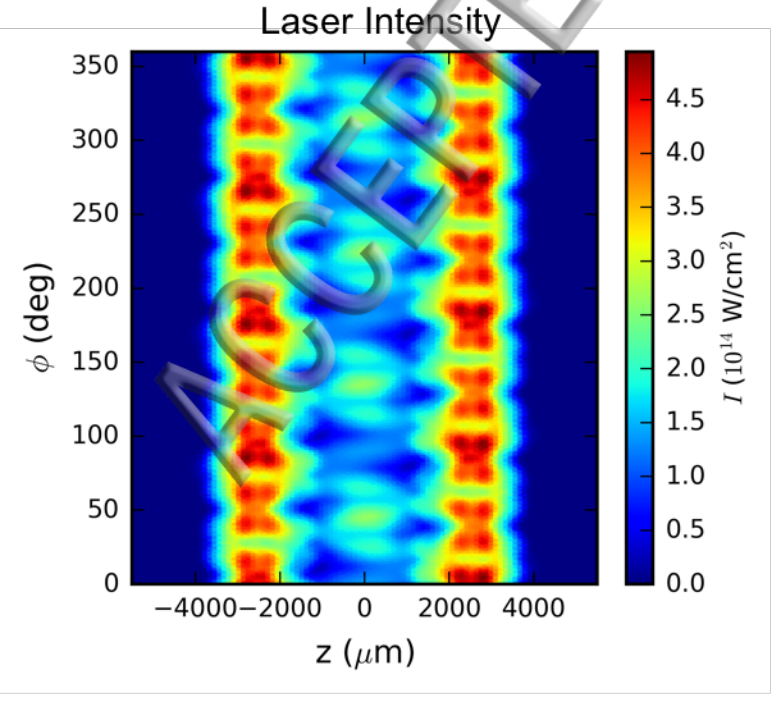
Laser Intensity
350
300
250
200
150
100
50
0
ϕ (deg)
−4000 −2000 0 2000 4000
z (μm)
4.5
4.0
3.5
3.0
2.5
2.0
1.5
1.0
0.5
0.0
I (10^{14} W/cm^2)

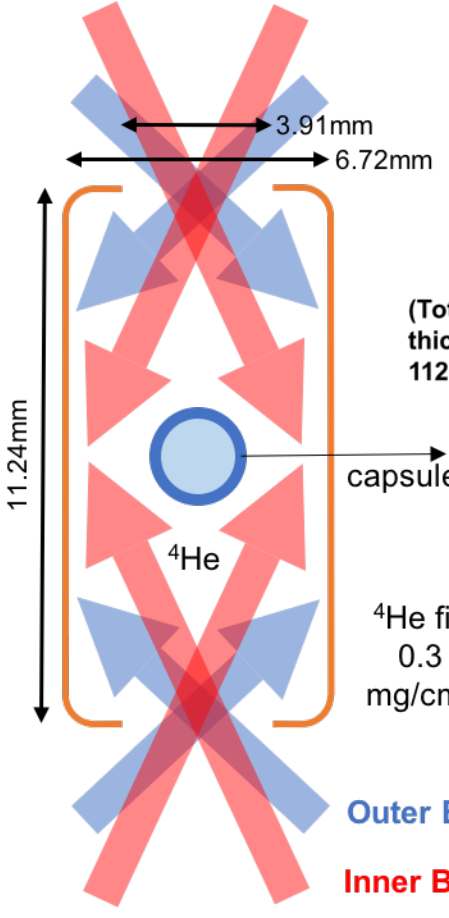
3.91mm
6.72mm
11.24mm
capsule
^{4}He
^{4}He fill
0.3
mg/cm^3
Outer Beams
Inner Beams

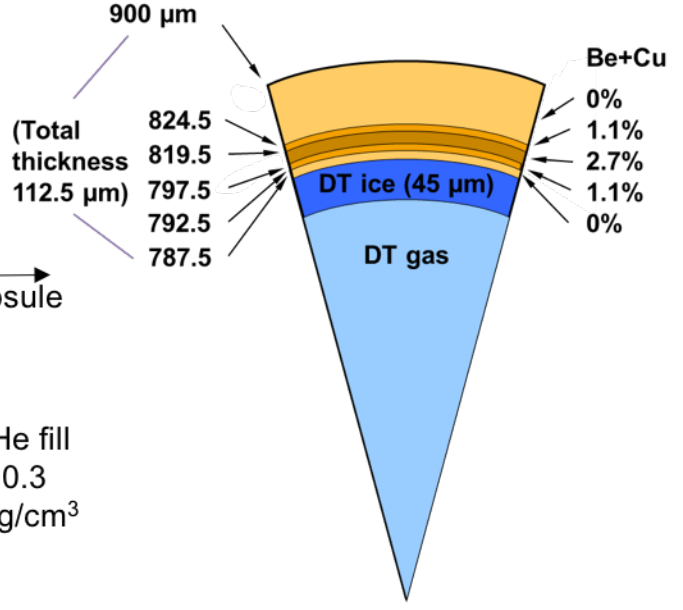
900 μm
(Total
thickness
112.5 μm)
824.5
819.5
797.5
792.5
787.5
Be+Cu
0%
1.1%
2.7%
1.1%
0%
DT ice (45 μm)
DT gas

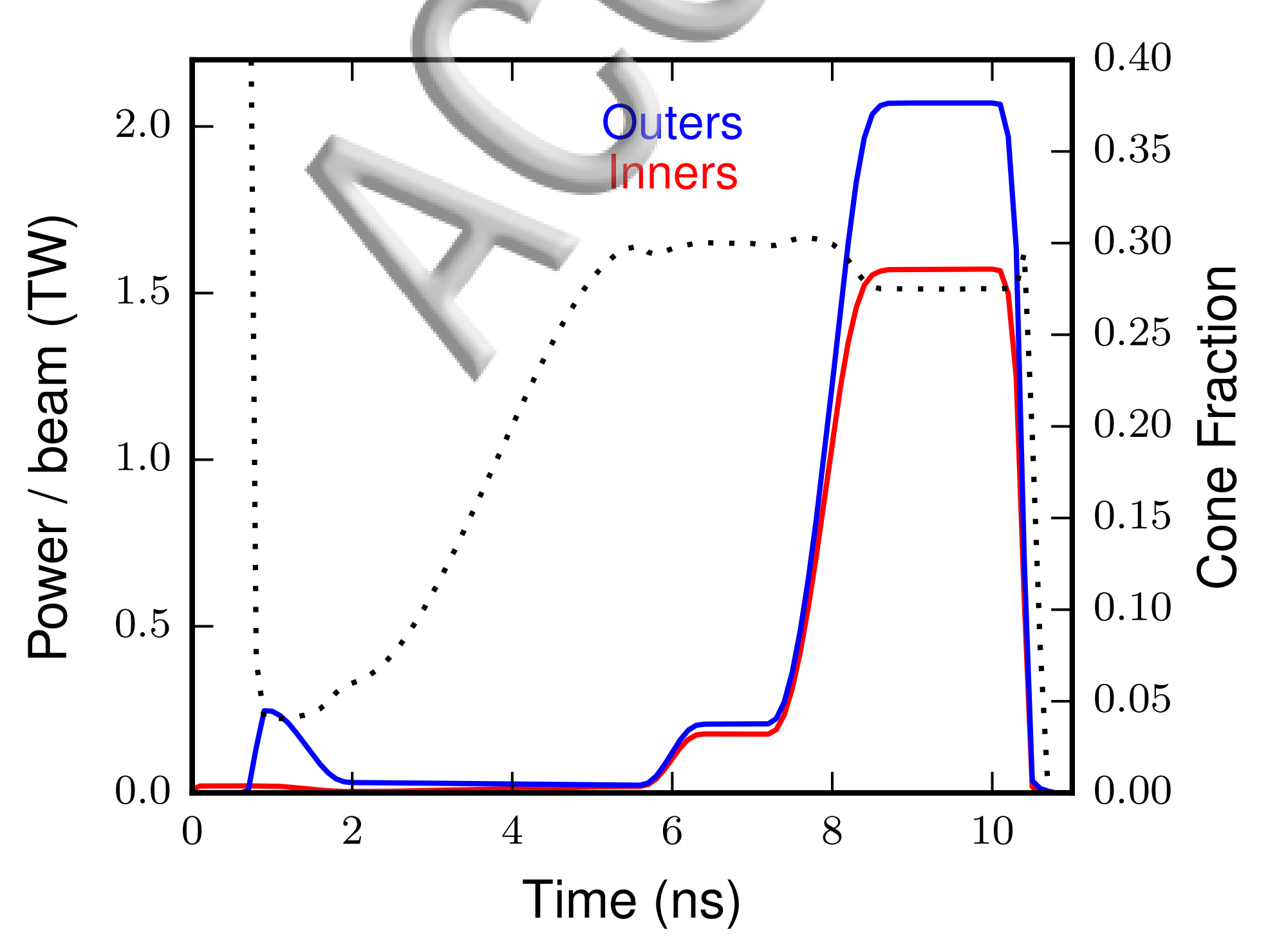
Outers
Inners
Power / beam (TW)
Cone Fraction
Time (ns)
0.0
0.5
1.0
1.5
2.0
0
2
4
6
8
10
0.00
0.05
0.10
0.15
0.20
0.25
0.30
0.35
0.40

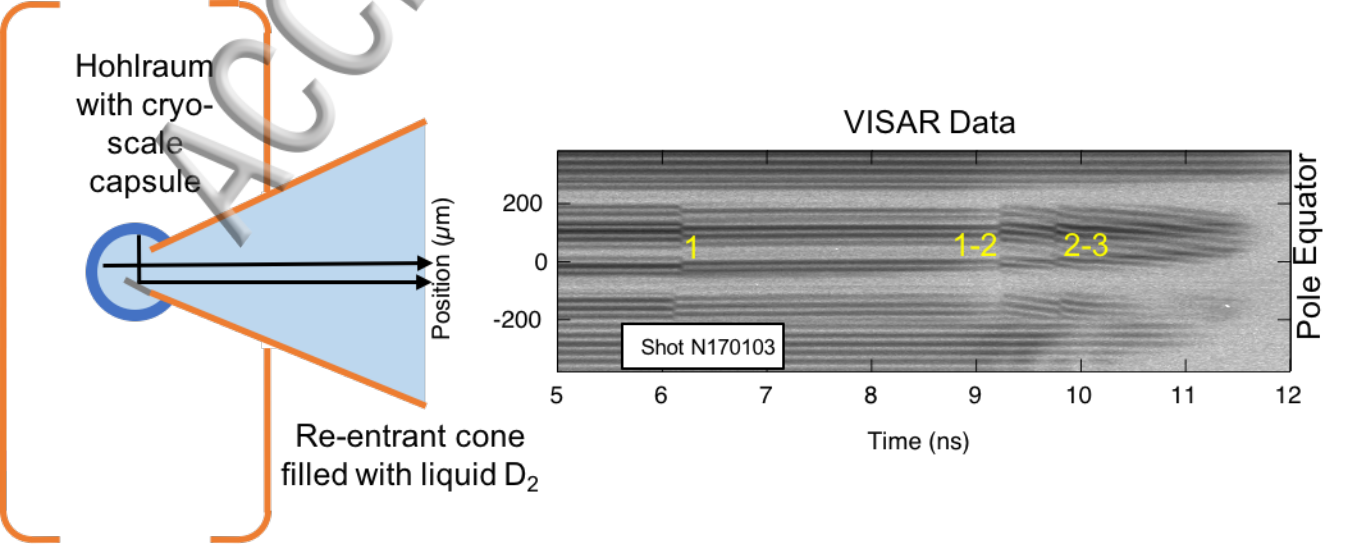
Hohlraum with cryo-scale capsule
Position (μm)
Re-entrant cone filled with liquid D_2
VISAR Data
200
0
-200
1
1-2
2-3
Shot N170103
Pole Equator
5
6
7
8
9
10
11
12
Time (ns)

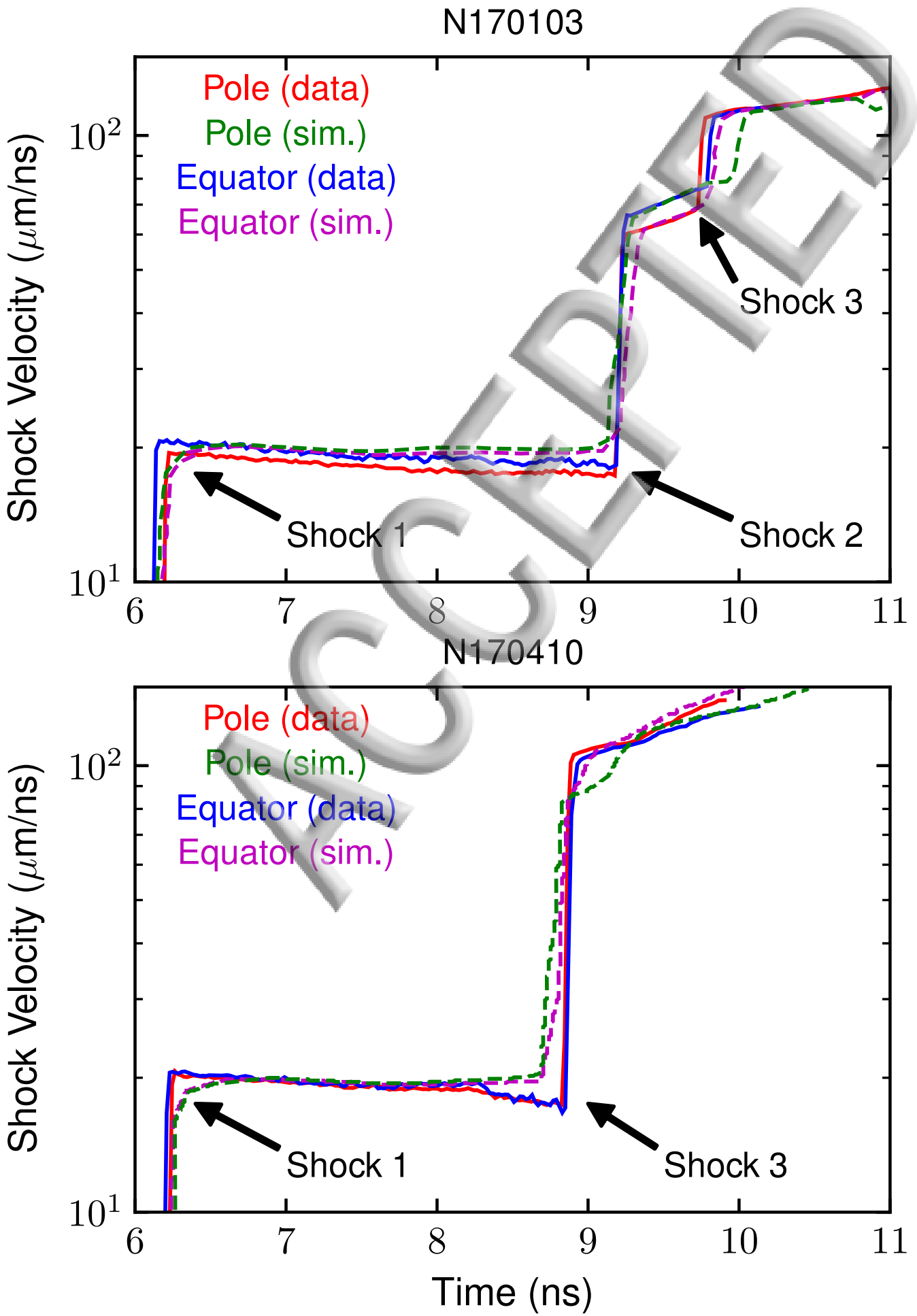
N170103
Pole (data)
Pole (sim.)
Equator (data)
Equator (sim.)
Shock 1
Shock 2
Shock 3
N170410
Pole (data)
Pole (sim.)
Equator (data)
Equator (sim.)
Shock 1
Shock 3
Shock Velocity (μm/ns)
Time (ns)
10^2
10^1
6
7
8
9
10
11

ACCEPTED

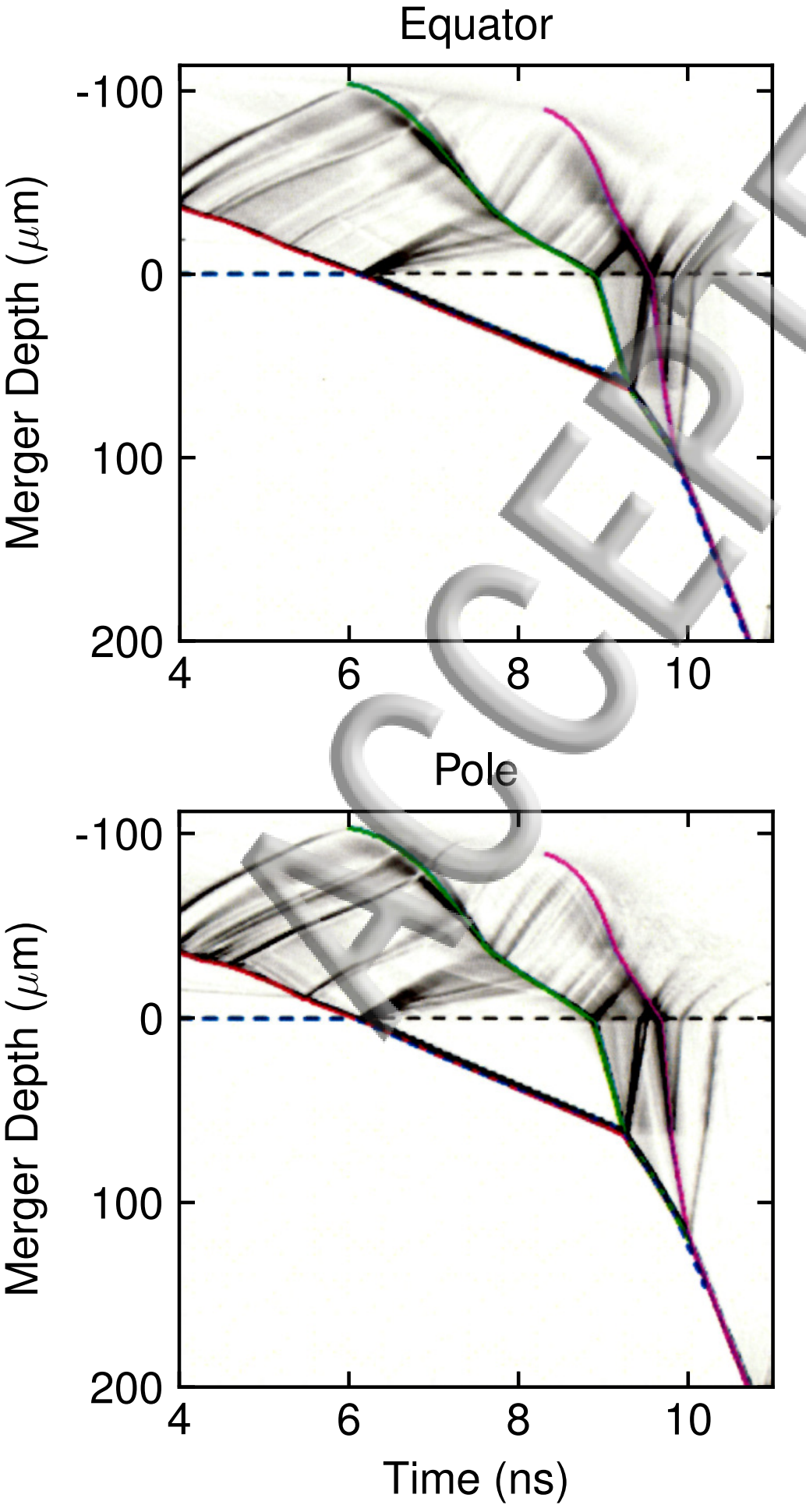

ACCEPTED

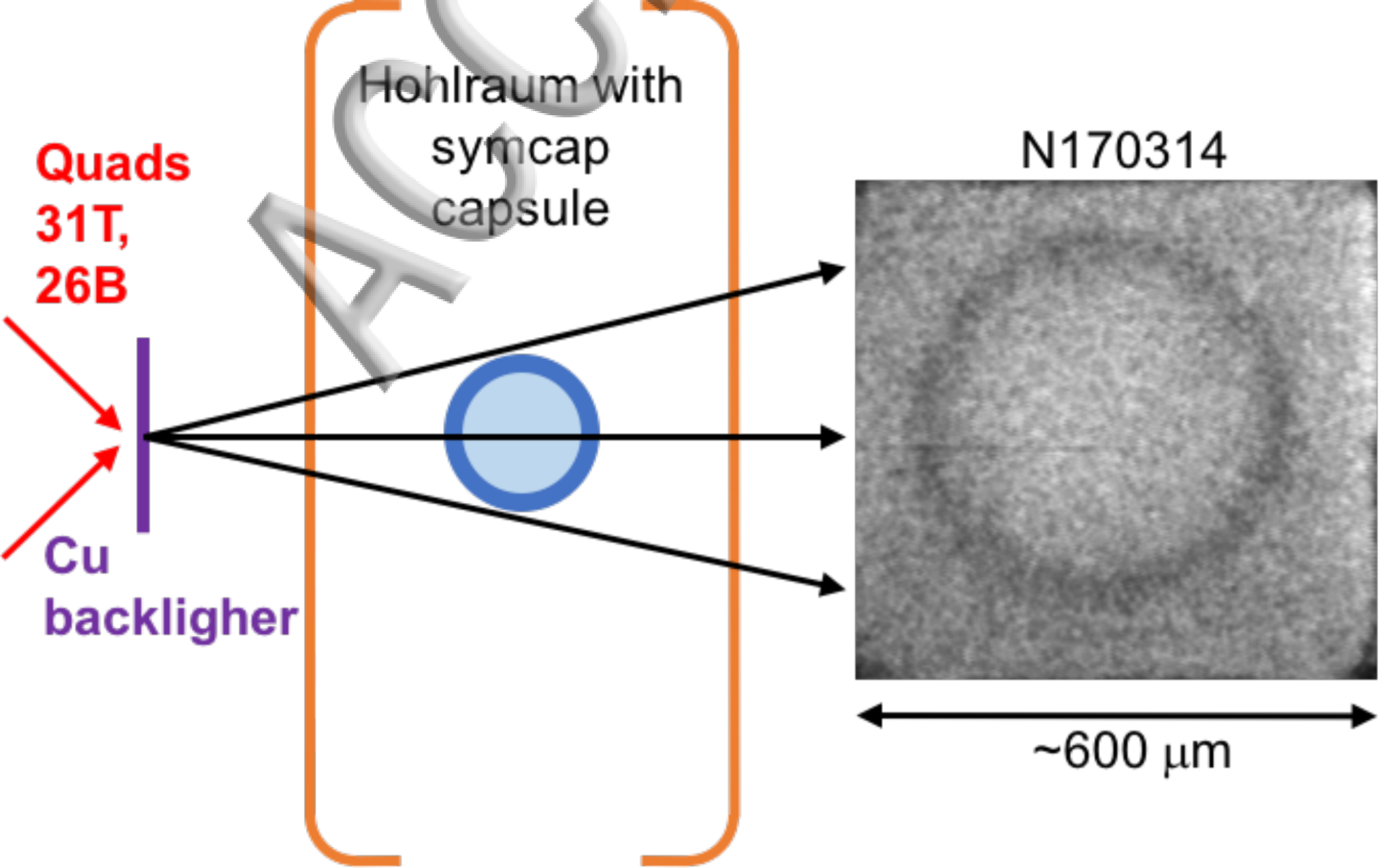
Hohlraum with
symcap
capsule
Quads
31T,
26B
Cu
backligher
N170314
~600 μm

ACCEPTED

0-0 HGXD

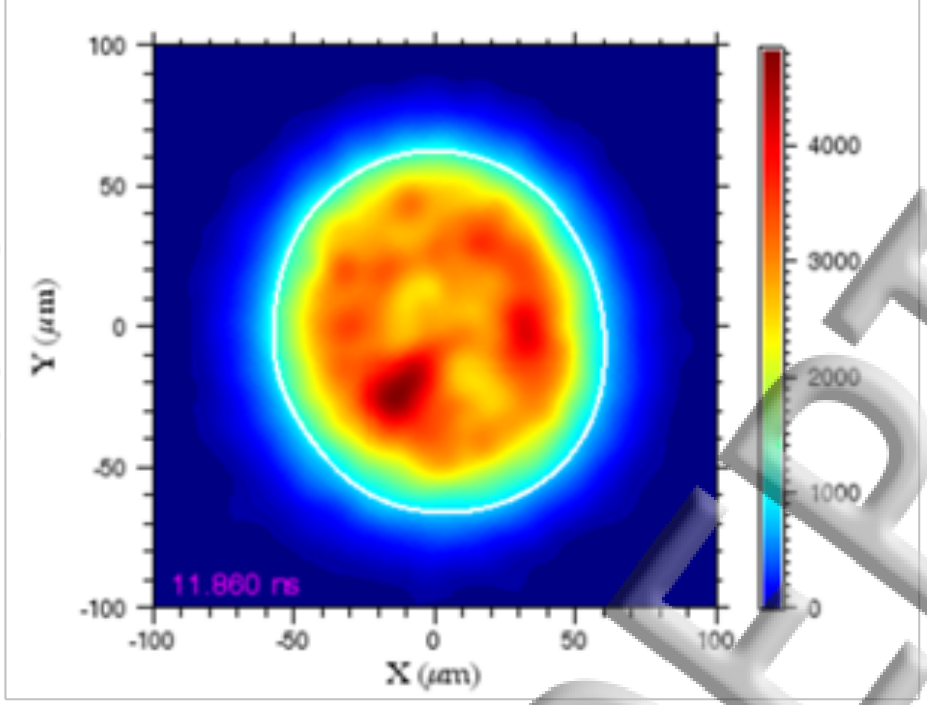

Shot N170327

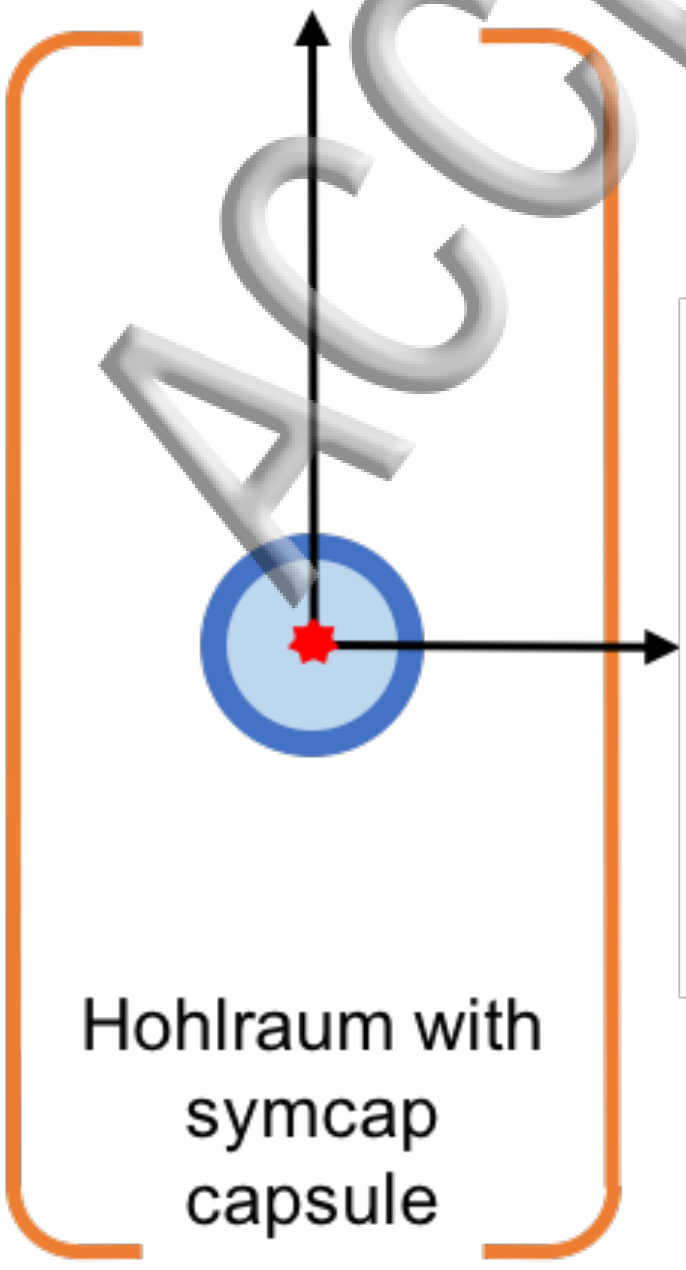

90-78 HGXD

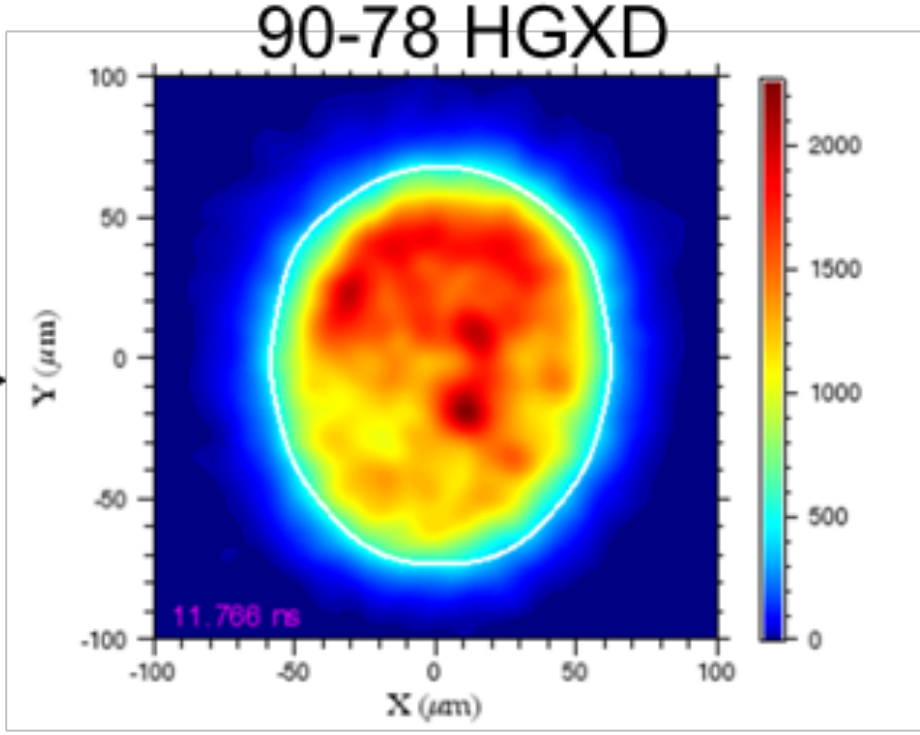

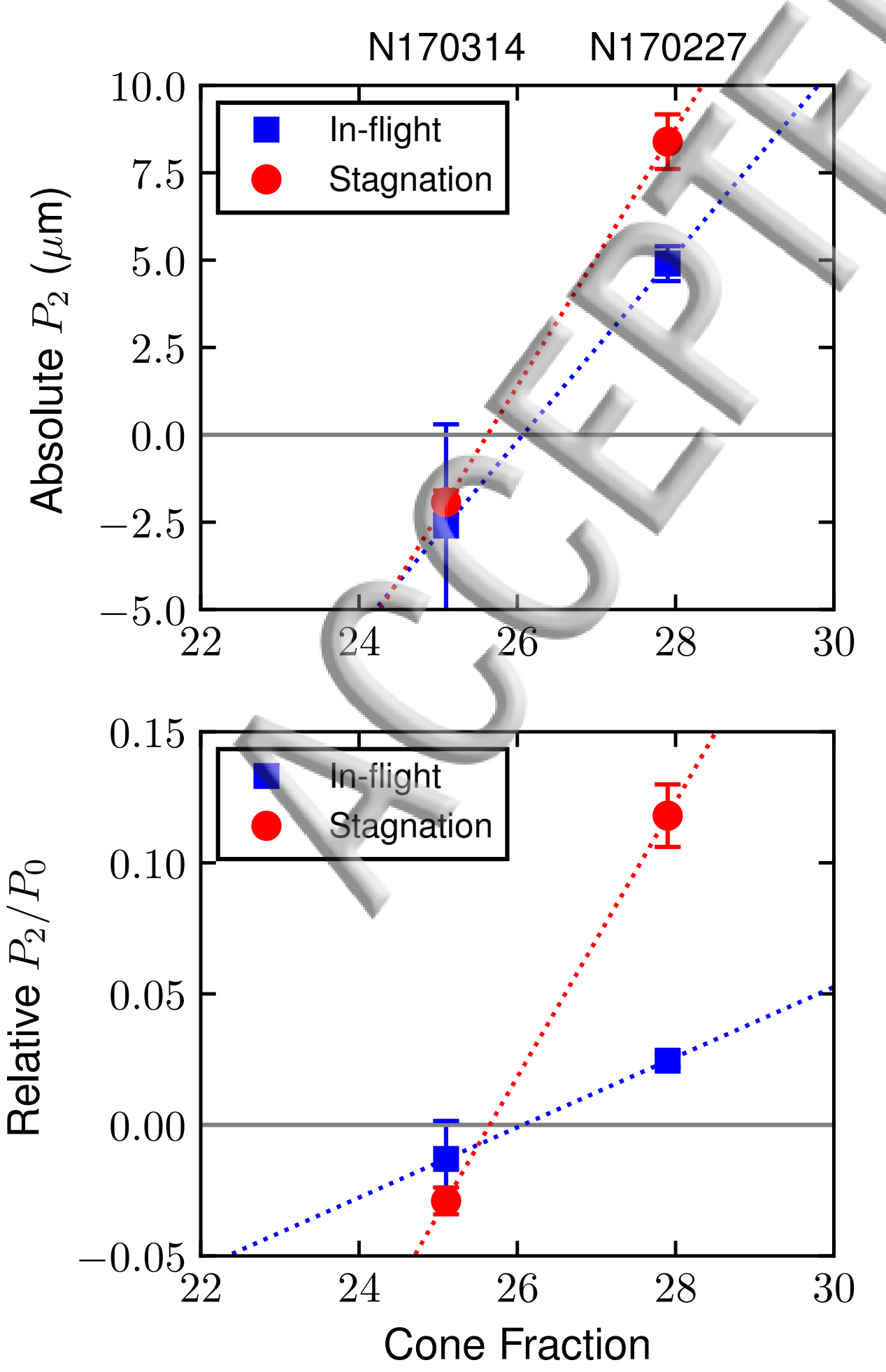
N170314
N170227
In-flight
Stagnation
Absolute P_2 (μm)
10.0
7.5
5.0
2.5
0.0
−2.5
−5.0
22
24
26
28
30
In-flight
Stagnation
Relative P_2/P_0
0.15
0.10
0.05
0.00
−0.05
22
24
26
28
30
Cone Fraction
ACCEPTED

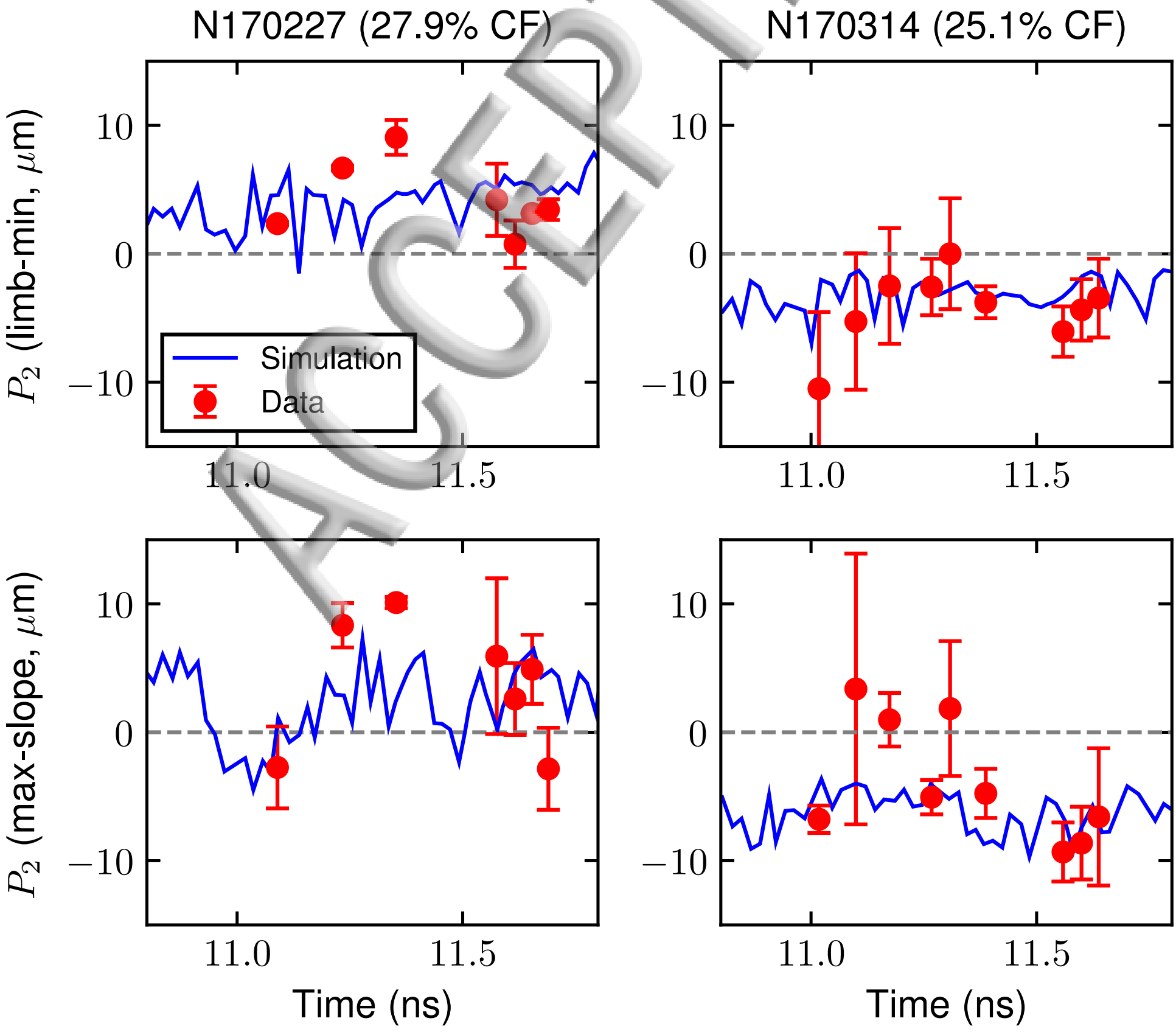
N170227 (27.9% CF)
N170314 (25.1% CF)
P_2 (limb-min, μm)
P_2 (max-slope, μm)
Simulation
Data
10
0
−10
11.0
11.5
Time (ns)
ACCEPTED

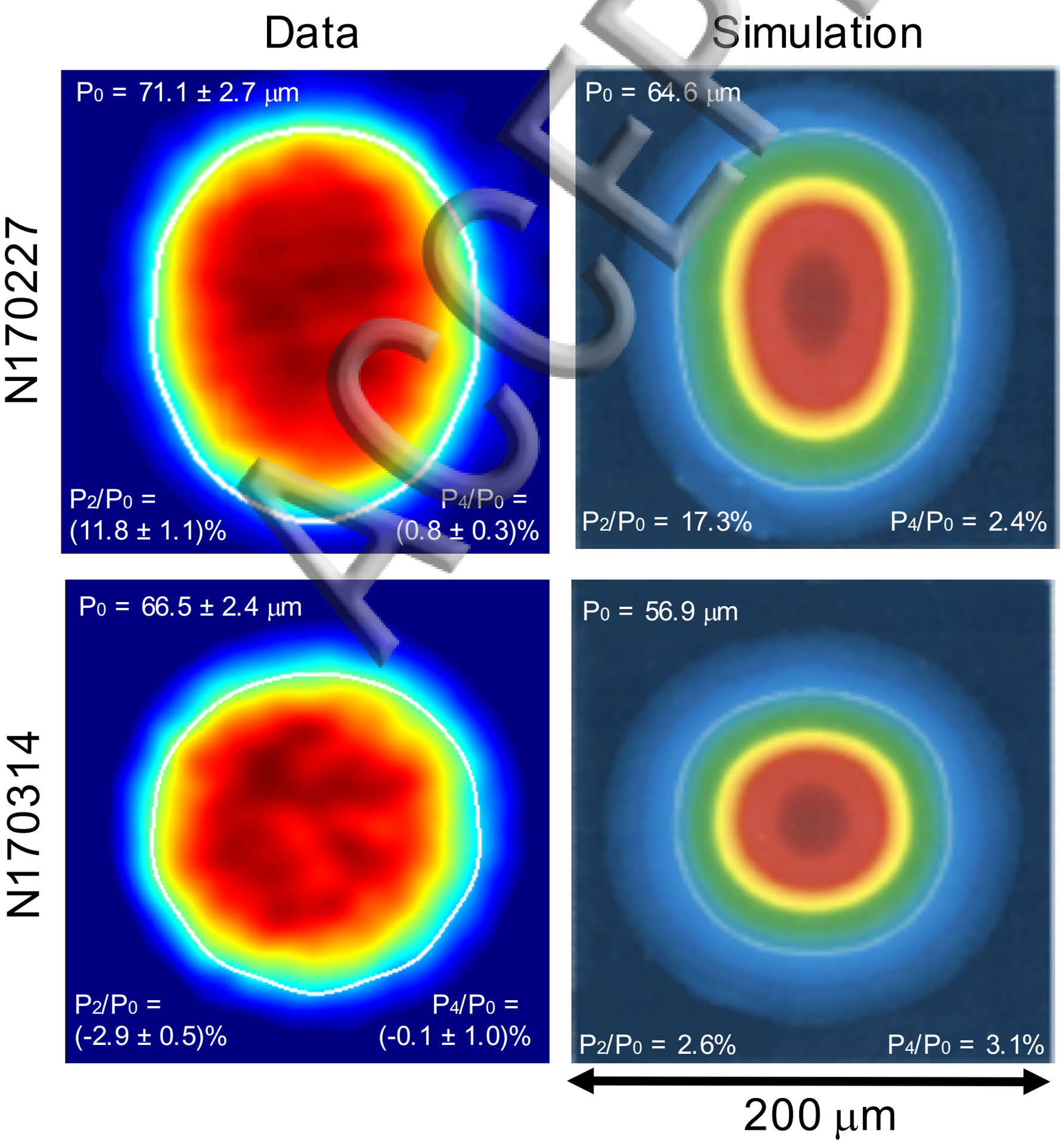
Data
Simulation
N170227
N170314
P0 = 71.1 ± 2.7 μm
P2/P0 = (11.8 ± 1.1)%
P4/P0 = (0.8 ± 0.3)%
P0 = 64.6 μm
P2/P0 = 17.3%
P4/P0 = 2.4%
P0 = 66.5 ± 2.4 μm
P2/P0 = (-2.9 ± 0.5)%
P4/P0 = (-0.1 ± 1.0)%
P0 = 56.9 μm
P2/P0 = 2.6%
P4/P0 = 3.1%
200 μm

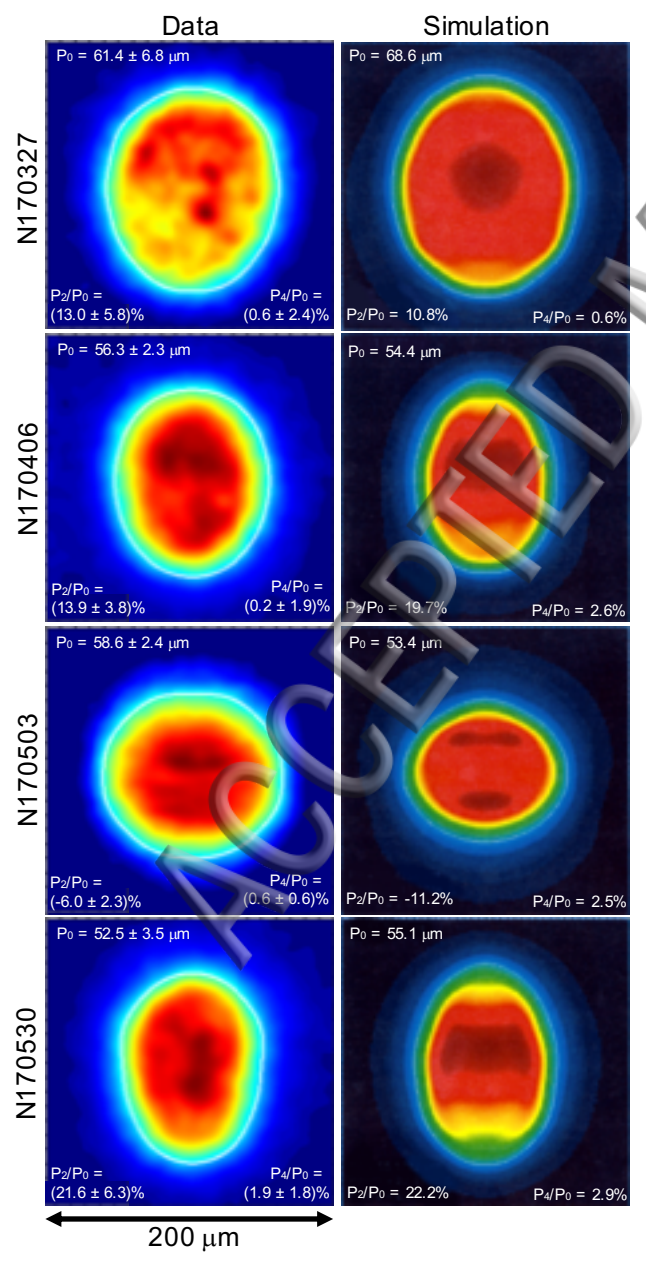
Data
Simulation
N170327
P0 = 61.4 ± 6.8 μm
P2/P0 = (13.0 ± 5.8)%
P4/P0 = (0.6 ± 2.4)%
P0 = 68.6 μm
P2/P0 = 10.8%
P4/P0 = 0.6%
N170406
P0 = 56.3 ± 2.3 μm
P2/P0 = (13.9 ± 3.8)%
P4/P0 = (0.2 ± 1.9)%
P0 = 54.4 μm
P2/P0 = 19.7%
P4/P0 = 2.6%
N170503
P0 = 58.6 ± 2.4 μm
P2/P0 = (-6.0 ± 2.3)%
P4/P0 = (0.6 ± 0.6)%
P0 = 53.4 μm
P2/P0 = -11.2%
P4/P0 = 2.5%
N170530
P0 = 52.5 ± 3.5 μm
P2/P0 = (21.6 ± 6.3)%
P4/P0 = (1.9 ± 1.8)%
P0 = 55.1 μm
P2/P0 = 22.2%
P4/P0 = 2.9%
200 μm
ACCEPTED

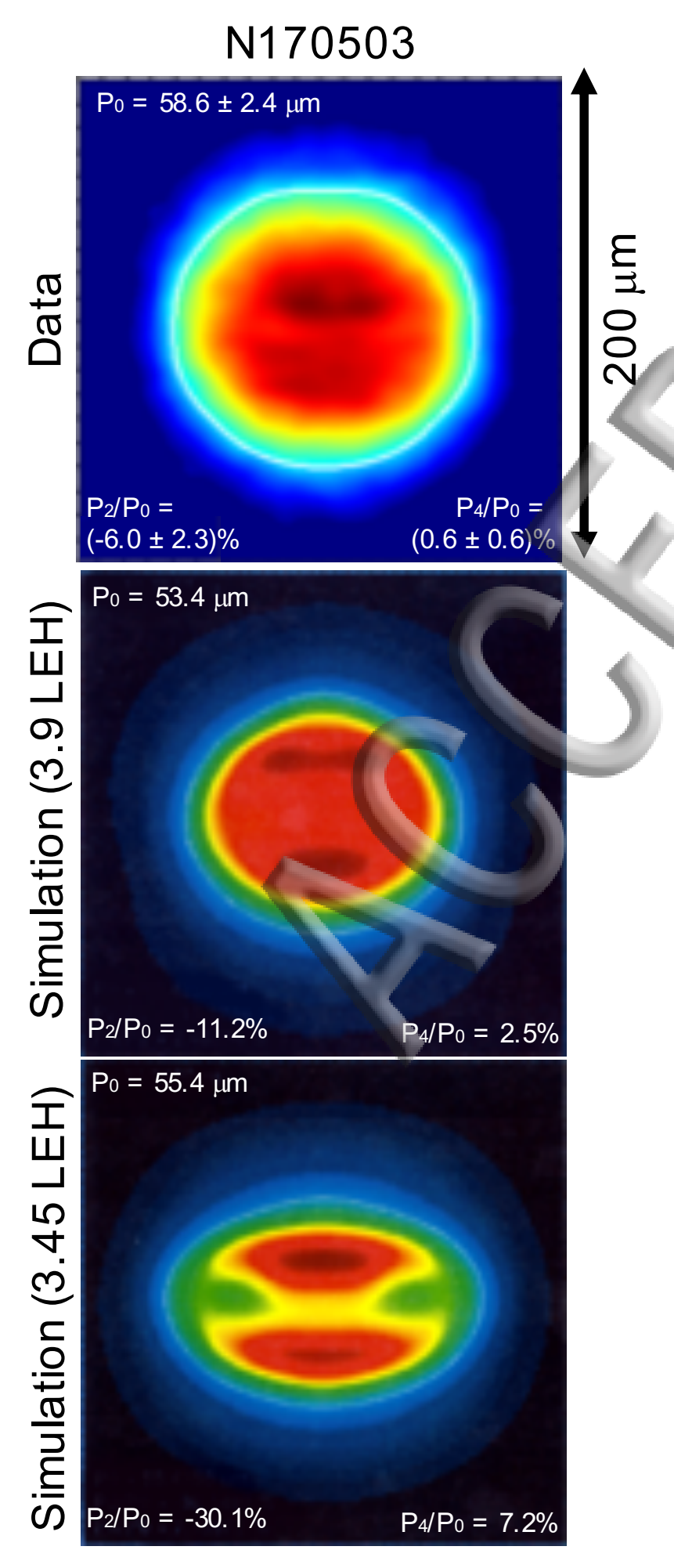
N170503
Data
P0 = 58.6 ± 2.4 μm
P2/P0 = (-6.0 ± 2.3)%
P4/P0 = (0.6 ± 0.6)%
200 μm
Simulation (3.9 LEH)
P0 = 53.4 μm
P2/P0 = -11.2%
P4/P0 = 2.5%
Simulation (3.45 LEH)
P0 = 55.4 μm
P2/P0 = -30.1%
P4/P0 = 7.2%

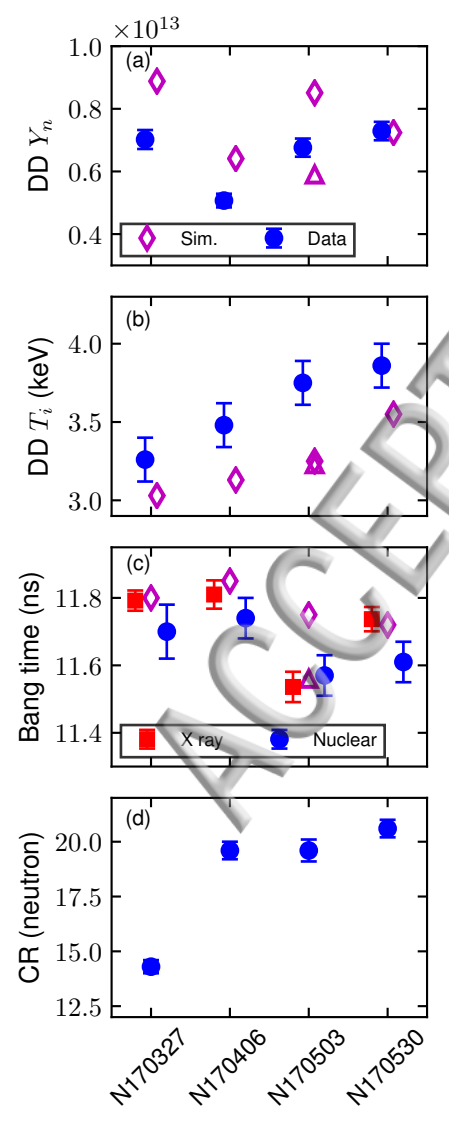
×10^13
1.0
0.8
0.6
0.4
(a)
DD Y_n
Sim.
Data
(b)
DD T_i (keV)
4.0
3.5
3.0
(c)
Bang time (ns)
11.8
11.6
11.4
X ray
Nuclear
(d)
CR (neutron)
20.0
17.5
15.0
12.5
N170327
N170406
N170503
N170530

N170327

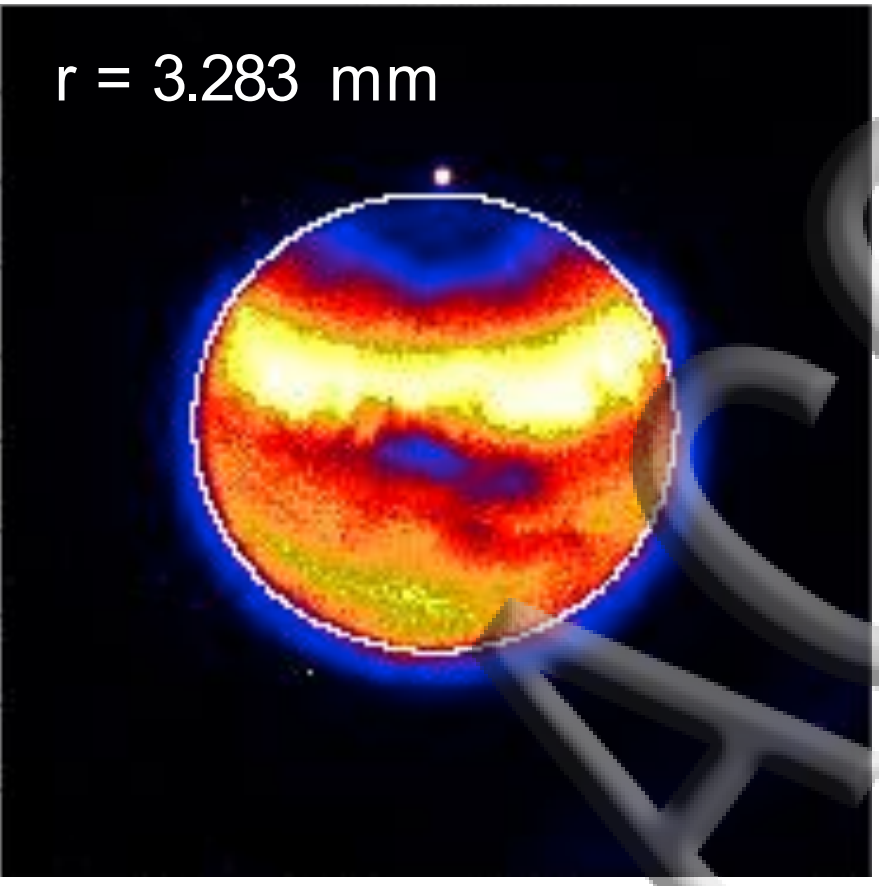

N170406

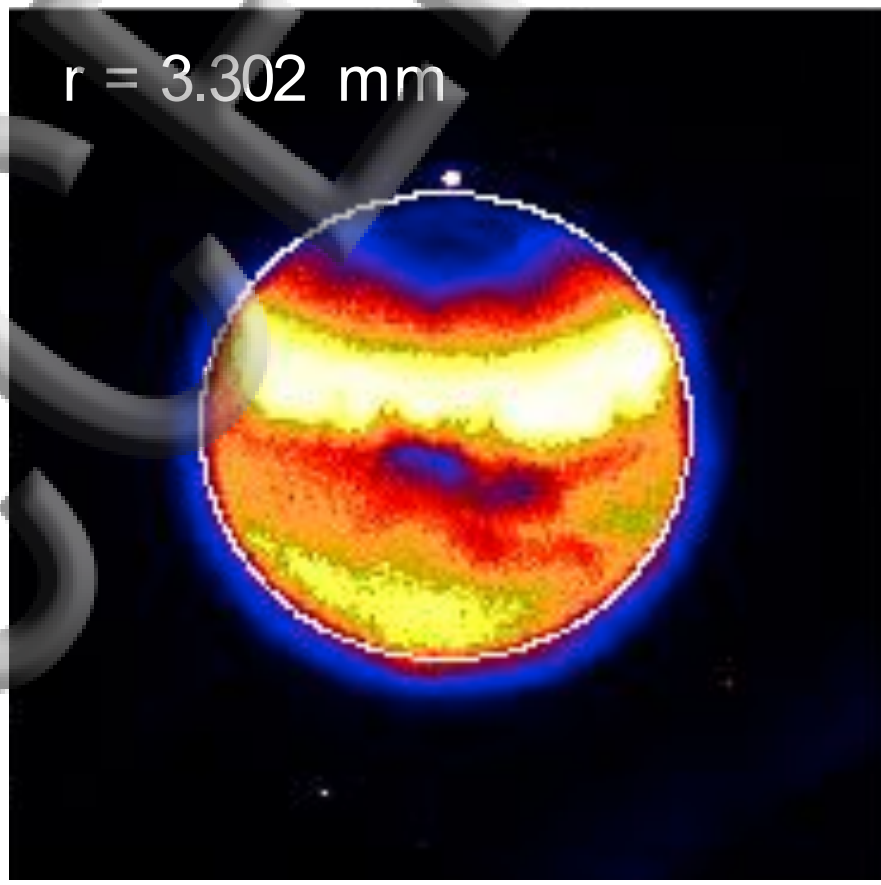

N170503

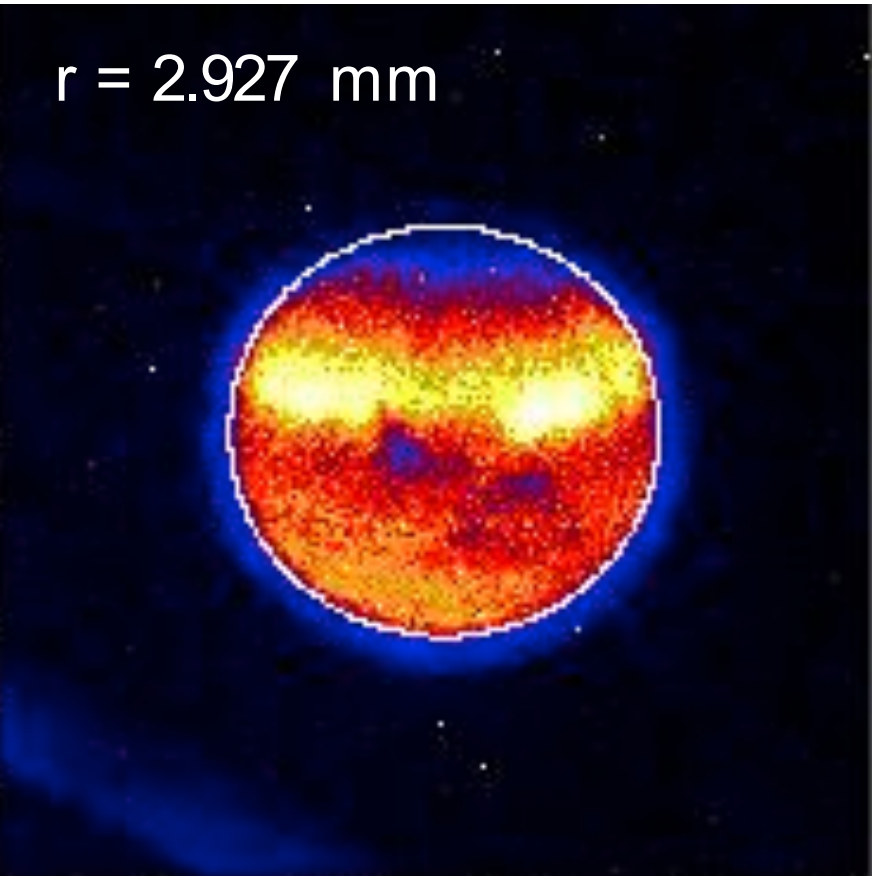

N170530

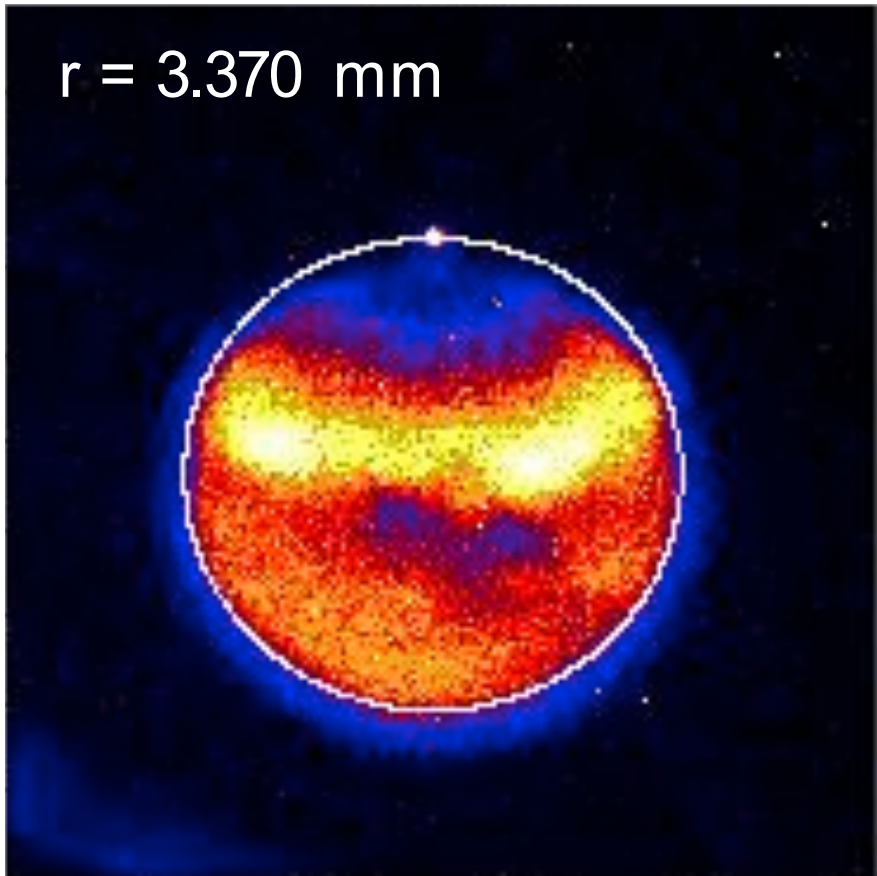

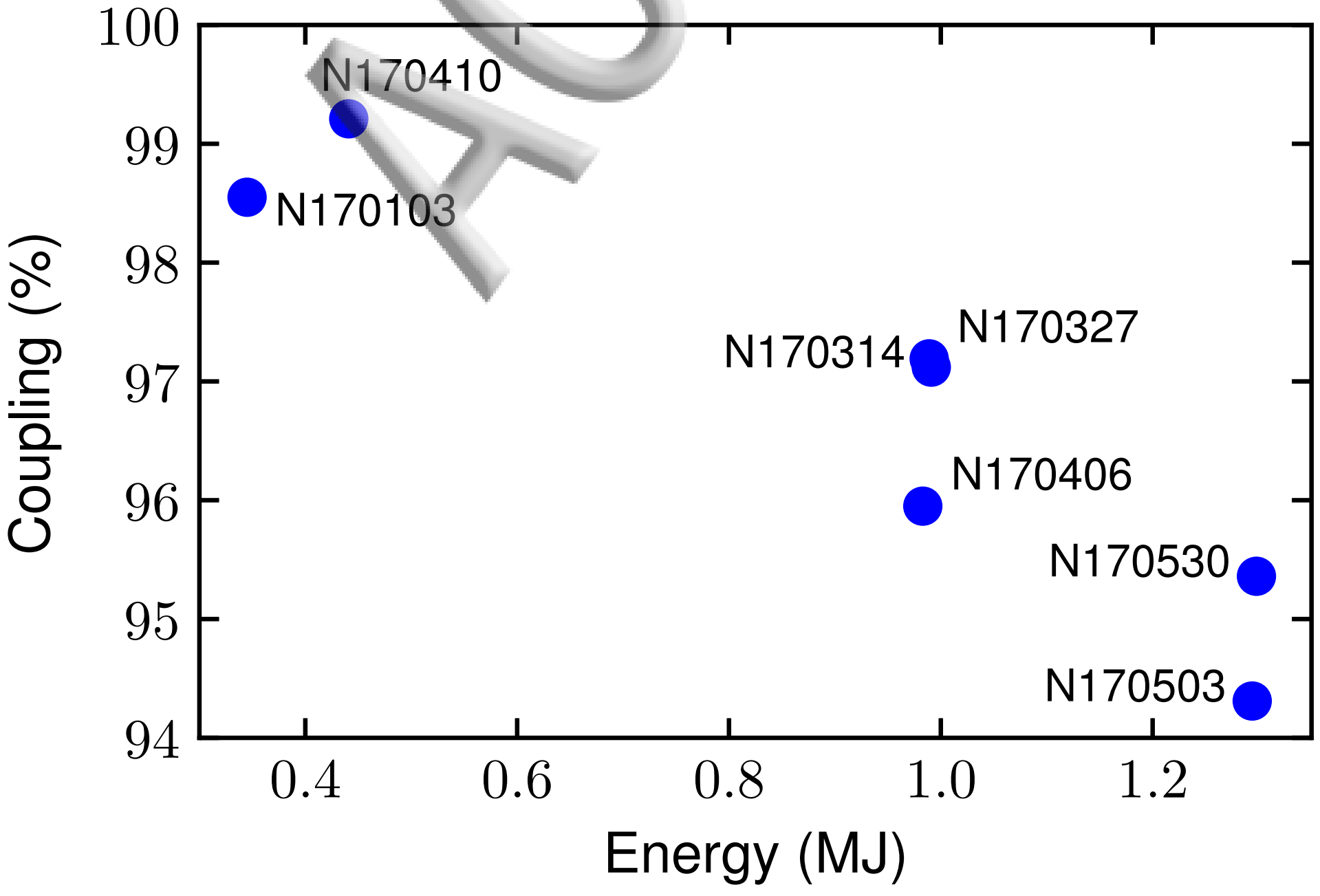
100
99
98
97
96
95
94
Coupling (%)
0.4
0.6
0.8
1.0
1.2
Energy (MJ)
N170410
N170103
N170314
N170327
N170406
N170530
N170503

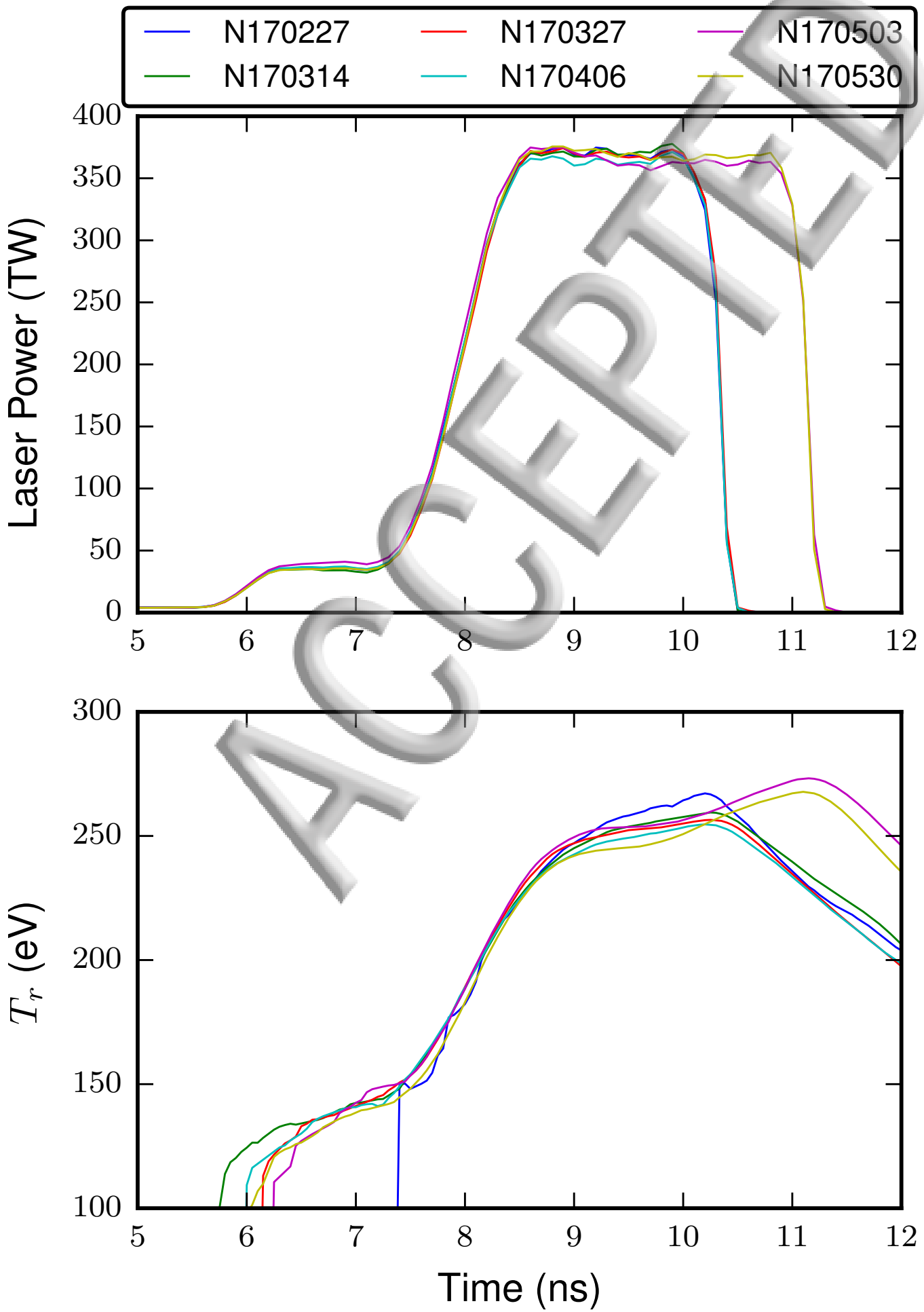
N170227
N170314
N170327
N170406
N170503
N170530
Laser Power (TW)
400
350
300
250
200
150
100
50
0
5
6
7
8
9
10
11
12
T_r (eV)
300
250
200
150
100
5
6
7
8
9
10
11
12
Time (ns)

ACCEPTED

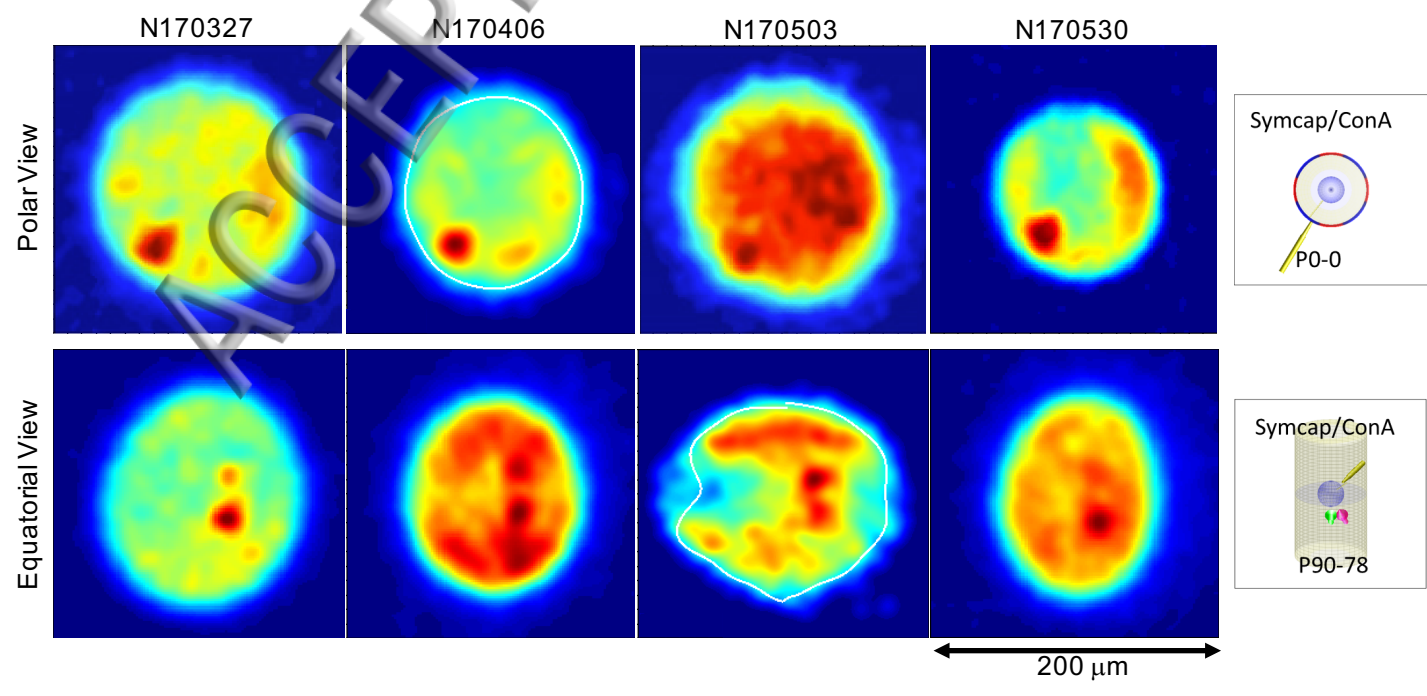
N170327
N170406
N170503
N170530
Polar View
Equatorial View
Symcap/ConA
P0-0
Symcap/ConA
P90-78
200 μm